Utrecht University

Classical Density Functional Theory

And the effect of dispersion forces on the electrochemical properties of room temperature ionic liquids

by

[Maarten Rottier m.k.rottier@students.uu.nl]

Abstract In this thesis the theoretical framework of classical density functional theory (DFT) will be examined. Density functional theory is a tool for determining the structural and thermodynamic properties inhomogeneous fluids. It predicts the existence of a functional of the particle density distributions. Functional minimization of this functional yields the equilibrium density profiles. Using a Picard-iteration scheme in *Matlab* we do this functional minimization for an ionic liquid in contact with a set of planar electrodes. We will examine the influence of dispersion forces on the shape of the surface charge density and differential capacitance. It turns out that the experimentally observed transition between a camel- and bell-shaped differential capacitance curve for increasing packing fractions is closely related to the strength of the dispersion forces in play. Dispersive attraction with the charged wall will at low surface charge result in an accumulation of ions, stabilizing the bell-shaped differential capacitance. If dispersion forces between the particles and the electrode surface are removed, ionic densities will be depleted in the vicinity of the electrode surface for low electrode potentials, leading to a drop in capacitance around zero surface charge.

Supervisors:

Prof. dr. René van Roij
Institute for Theoretical Physics

Peter Cats, MSc
Institute for Theoretical Physics

Department of Physics
Bachelor Thesis

Acknowledgements

I want to thank René and Peter for their endless enthusiasm and encouragement during the weekly meetings. Special thanks to Peter for spending many hours patiently helping me with Matlab. I want to thank 'nature' for the great 4 years of drinking coffee and having fruitful discussions.

Contents

List of Figures

Chapter 1

Introduction

When a charged entity like an electrode is placed in a solution containing mobile ions, a so called electric double (EDL) forms. Ions with opposite charge as to the electrode are attracted and those with the same sign are repelled. These ions are commonly referred to as counter-ions and co-ions, respectively. Together they form a diffuse cloud in order to screen of the charge of the immersed object. These electric double layers pop up all over physics and in technological applications [1]. Understanding the physics at the electrode interface will be of great importance in solving many challenges that mankind faces these days.

Maybe the greatest of all these challenges is solving the imminent energy crisis. With a big part of the third world going through the phase of industrializing their economies the global need for energy is bound to increase enormously. At the same time we are becoming increasingly aware of the harm carbon emission, caused by burning fossil fuels, is doing to our planet. Increasing and at the same time decarbonizing the global energy supply asks for an enormous increase in clean energy sources.

A part of the solution could be provided by so-called blue energy harvesting devices. When sea water (high concentration of ions) mixes with fresh water (low concentration of ions) free energy dissipates. Considering how much fresh water flows into the sea, the harvesting of this energy could play a significant role as part of the solution to the aforementioned energy problem. A promising technique for harvesting blue energy makes use of the charging and discharging of porous carbon electrodes in salt and fresh water, respectively. In order to understand these processes and overcome the technological challenges in building blue energy harvesting devices, it is of great importance to understand the EDL properties of carbon electrodes in contact with salt water [2].

Arguably as important as finding new sources of energy is the improvement of renewable sources that have been around for decades, as well as improving energy storage devices. This is one of the places where so called ionic liquids can play an important role [3, 4]. Ionic liquids are liquids consisting merely of ions. Roughly, they can be divided into two groups. Room temperature ioniq liquids (RTIL's) have melting points below 100 °C, and molten salts have melting points above 100 °C. Ionic liquids exhibiting volatility and high electrochemical and thermal stability create possibilities for improving electrolyte batteries, solar cells and super-capacitors. In order to realize this technologically it is important to have a solid understanding of the physical processes of IL's in contact with charged surfaces.

In this thesis we will explore the mathematics of classical density functional theory. This mathematical framework is gaining increased interest from the scientific community for its wide applicability in various problems and its straightforward manner of implementing external potentials. In the case of ions in contact with charged electrode surfaces this theory will predict both structural and thermodynamic properties. After the theory has been developed we will use this framework to examine the effect of dispersion forces on the structure and electrochemical properties of the electric double layer that forms when RTIL's get in contact with planar electrode surfaces.

Chapter 2

Classical Density Functional Theory

Classical Density Functional Theory (DFT) is a theoretical framework for determining the thermodynamic properties of *inhomogeneous* fluids. Within the DFT framework, the degrees of freedom one has to deal with is reduced significantly with respect to the partition function as described by statistical physics. Density functional theory starts from a microscopic basis, the particle Hamiltonian, and is introduced in grand canonical setting. The key result is that the grand potential of an inhomogeneous fluid is a functional of the particle density. Functional minimization of the grand potential with respect to the density yields the physical (equilibrium) density profile. When evaluated at this equilibrium density distribution this functional yields the grand potential. Structural and thermodynamic properties follow from the density and grand potential, respectively. The development of this section is based on the relevant sections on DFT in [5–10].

Like the title of this section is implying, we will consider classical density functional theory. The general framework of density functional theory, however, was first developed in a quantum mechanical setting. In 1964 Hohnenberg and Kohn realized that instead of solving the N-particle Schrödinger equation to describe the ground state ($T = 0$) of an electron gas, it is possible to obtain all information of the ground state from the electron density distribution [11]. They managed to establish existence of a ground state energy functional that can be written as a functional of the density distribution. Next, they went on and noted that the *physical* density distribution minimizes this functional, and that *every* other density distribution yields a greater ground state energy than the physical distribution. Not long after that Mermin managed to prove that this framework also holds for systems with $T > 0$. After that it did not take too long for people to apply this powerful tool in the classical physics realm. While not the first one to pioneer this subject, Evans was the first who put the framework in the classical sense on a sound basis, reaching a wide audience [6]. The aim of this section is to introduce the framework of classical density functional theory. We will establish the existence and certain uniqueness properties of a grand potential functional and we will discuss how to arrive at the fundamental equations describing inhomogeneous fluids. For a short introduction to some of the concepts needed we refer the reader to Appendix A, Appendix B and Appendix C. In these appendices the relevant concepts needed for the development of DFT, variational calculus, thermodynamics and statistical mechanics, respectively, are discussed.

2.1 One component mixtures

We start by considering a system consisting of N spherical particles with masses m. The particle positions are denotes by $\mathbf{r}_i$, and the momenta by $\mathbf{p}_i$. In this case the Hamiltonian of the system takes the following form

$$H_N = K + \Phi + \mathcal{V}, \tag{2.1}$$

with K, Φ and $\mathcal{V}$ denoting the kinetic energy, the potential energy due to inter-particle interactions (not necessarily pairwise additive) and the potential energy due to some (at this point unspecified) external potential, respectively,

$$K = \sum_{i=1}^{N} \frac{\mathbf{p}_i}{2m}, \tag{2.2}$$

$$\Phi = \Phi\left(\mathbf{r}_1 \cdots \mathbf{r}_N\right), \tag{2.3}$$

$$\mathcal{V} = \sum_{i=1}^{N} V_{ext}\left(\mathbf{r}_i\right). \tag{2.4}$$

We note that the demand for the system to be enclosed within a certain volume V is met by putting this constraint in $\mathcal{V}$. With this expression for the Hamiltonian the equilibrium distribution Eq. (C.14) becomes

$$f_0(\mathbf{r}^N, \mathbf{p}^N, N) = \frac{1}{\Xi} \exp\left[\beta(\mu N - H_N)\right]. \tag{2.5}$$

The grand canonical partition sum Eq. (C.15) reads

$$\Xi = \sum_{N=0}^{\infty} \frac{1}{N! h^{3N}} \int d\mathbf{p}_1 \cdots d\mathbf{p}_N d\mathbf{r}_1 \cdots d\mathbf{r}_N \exp\left[\beta(\mu N - H_N\right]. \tag{2.6}$$

For convenience we will define the *classical trace* Tr_{cl} as the sum over N and the integral over the momenta and positions of the particles

$$\mathrm{Tr}_{cl} \equiv \sum_{N=0}^{\infty} \frac{1}{N! h^{3N}} \int d\mathbf{p}_1 \cdots d\mathbf{p}_N d\mathbf{r}_1 \cdots d\mathbf{r}_N. \tag{2.7}$$

In principle Ξ contains all the equilibrium thermodynamics of the system. The problem is that for all but a handful of (easy) potentials it is not possible to calculate, or even approximate, Ξ. In the DFT framework it is somewhat easier to make approximations then to make immediate approximations for the partition sum.

The density operator (or the particle distribution function) $\widehat{\rho}(\mathbf{r})$ is defined as

$$\widehat{\rho}(\mathbf{r}) = \sum_{i=1}^{N} \delta(\mathbf{r} - \mathbf{r}_i). \tag{2.8}$$

This function counts the amount of particles concentrated at a particular position $\mathbf{r}$ in space. Since every particle has to be somewhere, it is readily seen that upon integration of $\widehat{\rho}$ over the whole of space you obtain the total number of particles N,

$$\int d\mathbf{r} \sum_{i=1}^{N} \delta(\mathbf{r} - \mathbf{r}_i) = \sum_{i=1}^{N} \int d\mathbf{r} \delta(\mathbf{r} - \mathbf{r}_i) = N. \tag{2.9}$$

Using the equilibrium probability density we can calculate ensemble averages $\langle \widehat{O} \rangle$ of operators O as

$$\mathrm{Tr}_{cl} f_0 \widehat{O} \equiv \langle \widehat{O} \rangle. \tag{2.10}$$

As a side note, there is no deeper meaning to the notion of an operator here. This is the rudiment of a theory developed in quantum mechanical setting, where one extensively deals with operators. Of particular interest will be the equilibrium density $\rho_0(\mathbf{r})$ of the system

$$\rho_0(\mathbf{r}) = \mathrm{Tr}_{cl} f_o \widehat{\rho}(\mathbf{r}). \tag{2.11}$$

2.1.1 The grand potential functional

Analogously to the original paper by Mermin [12], we consider the following functional on the space of normalized phase space distribution functions corresponding to the Hamiltonian Eq. (2.1), which we will refer to as the grand potential functional

$$\Omega[f] = \mathrm{Tr}_{cl} f(H_N - \mu N + \beta^{-1} \ln f). \tag{2.12}$$

On first sight this functional has already an important and remarkable property. Namely when plugging in $f = f_0$ you obtain the grand potential

$$\begin{aligned}
\Omega[f_0] &= \mathrm{Tr}_{cl} f_0 (H_N - \mu N + \beta^{-1} \ln f_0) \\
&= \mathrm{Tr}_{cl} f_0 (H_N - \mu N + \beta^{-1} \ln [\frac{1}{\Xi} \exp [\beta(\mu N - H_N]]) \\
&= \mathrm{Tr}_{cl} f_0 (H_N - \mu N + \beta^{-1} [\beta(\mu N - H_N) - \ln \Xi]) \\
&= \mathrm{Tr}_{cl} f_0 (-\beta^{-1} \ln \Xi) \\
&= -\beta^{-1} \ln \Xi.
\end{aligned} \tag{2.13}$$

Where in the last line it was used that $\mathrm{Tr}_{cl} f_0 = 1$. The second property, that takes a little bit more work to establish, will be that f_0 actually *minimizes* $\Omega[f]$. In other words, for *any* other normalized phase space distribution function f we have that $\Omega[f] > \Omega[f_0]$. In order to prove this fact we make use of the so called Gibbs-inequality from probability theory.

Theorem 2.1.1. *Let $A(x^N)$ and $B(x^N)$ be two non-negative functions satisfying the normalization condition $\int dx^N A(x^N) = \int dx^N B(x^N) = 1$. Then the following inequality, known as the Gibbs-inequality, holds:*

$$\int dx^N A(x^N)(\log A(x^N) - \log B(x^N)) > 0, A(x^N) \neq B(x^N). \tag{2.14}$$

Here $x^N = (x_1 \cdots x_n)$ is an arbitrary set of variables.

Proof. We define $f(y) = y \ln y - y + 1$. We observe that $f'(y) = \ln y$. Hence $f'(y) = 0$ if and only if $y = 1$. Performing a second derivative test we observe that $f''(y) = \frac{1}{y} > 0$ for all $y \in \mathbb{R}^+$, hence the extremum at $y = 1$ is a minimum. Some further analysis by taking limits shows that this minimum is global, see fig. 2.1. We can conclude that for all $y \in \mathbb{R}^+, f(1) \leq f(y)$ implying that $y \ln y - y + 1 \geq 0$.

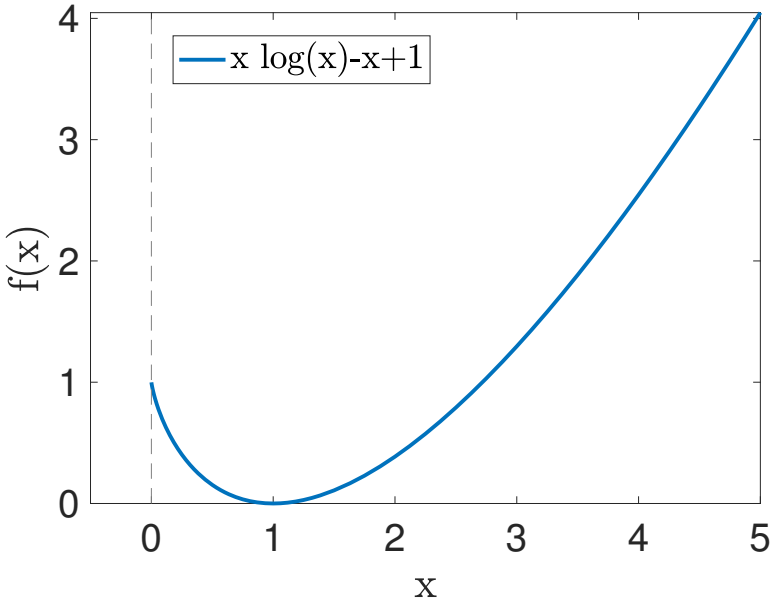

Figure 2.1: The function $f(x) = x \log(x) - x + 1$ for $x \geq 0$. Clearly, f reaches a global minimum at $x = 1$.

Now we write Eq. (2.14) as:

$$\begin{aligned}
\int dx^N A(x^N)(\log A(x^N) - \log B(x^N)) &= \int dx^N A(x^N) \log \frac{A(x^N)}{B(x^N)} \\
&= \int dx^N B(x^N) \left(\frac{A(x^N)}{B(x^N)} \log \frac{A(x^N)}{B(x^N)} \right) \\
&= \int dx^N B(x^N) \left(\frac{A(x^N)}{B(x^N)} \log \frac{A(x^N)}{B(x^N)} + 1 - \frac{A(x^N)}{B(x^N)} \right) \\
&\geq 0
\end{aligned} \tag{2.15}$$

Where in the last line we have used the fact deduced above with the substitution $y = \frac{A(x^N)}{B(x^N)}$ in combination with the fact that the probability distribution $B(x^N)$ is normalized. □

Now we can use the Gibbs inequality to prove that the equilibrium distribution is the one minimizing the grand potential functional. To do so we write Eq. (2.12) in the following suggestive way, using the facts that $H_N - \mu N = -kT \ln[\Xi f_0]$ and that f needs to be normalized

$$\begin{aligned}\Omega[f] &= \mathrm{Tr}_{cl} f(H_N - \mu N + \beta^{-1} \ln f) \\ &= \mathrm{Tr}_{cl} f(H_N - \mu N + \beta^{-1} \ln f + \beta^{-1} \ln f_0 - \beta^{-1} \ln f_0) \\ &= \Omega[f_0] + \beta^{-1} \mathrm{Tr}_{cl} f(\ln f - \ln f_0) \\ &\geq \Omega[f_0].\end{aligned} \tag{2.16}$$

Where we have used the Gibbs inequality in the last line to draw the desired conclusion.

2.1.2 Towards a functional of the particle density

At this point we have established the existence of a functional on the set of all normalized phase space distribution functions. However, like the name DFT suggests, we are on a quest to find a functional of the *density*. Something that will turn out to be extremely useful in the making of physical predictions. This section will be devoted to proving that the distribution function f in Eq. (2.12) is a unique functional of the one particle density $\rho(\mathbf{r}^N)$, which on its turn implies that the grand potential functional is a unique functional of the density. Following the development of [8, 9] the proof will be structured in three parts, two of which are rather trivial.

Theorem 2.1.2. *For a system with well defined temperature T, chemical potential μ, inter particle interaction Φ and external potential $\mathcal{V}$, the probability density f is a unique functional of the one particle density ρ.*

Proof. We begin by establishing the fact that the distribution function f is uniquely determined, for given T, μ, Φ by $\mathcal{V}$. Let $\mathcal{V} = \sum_{i=1}^{N} V_{ext}(\mathbf{r}_i)$ be any external potential, and let $\delta\mathcal{V}(\mathbf{r}_i)$ be any sufficiently smooth variation of $\mathcal{V}$. Let $\mathcal{V}' = \mathcal{V} + \delta\mathcal{V}$. Plugging in this variation the distribution f takes the following form

$$f' = \frac{\exp[-\beta^{-1} \sum_{i=0}^{N} \delta\mathcal{V}(\mathbf{r}_i)] \exp[-\beta^{-1}(H_N - \mu N)]}{\mathrm{Tr}_{cl} \exp[-\beta^{-1} \sum_{i=0}^{N} \delta\mathcal{V}(\mathbf{r}_i)] \exp[-\beta^{-1}(H_N - \mu N)]}. \tag{2.17}$$

Since $\delta\mathcal{V}$ only depends on the position of a particle in the system and not on the total number of particles there is no way to fine tune N in such a way that $f' = f$ for any nonzero variation $\delta\mathcal{V}$. In other words, the distribution function f is uniquely determined once $\mathcal{V}$ is determined.

By definition of ρ, Eq. (2.11), it is readily seen that the density distribution is a functional of f. Now we are ready for the non-trivial part of the proof, showing that f is a functional of ρ. It is sufficient to prove that for any two normalized distribution functions f, f' such that $f \neq f'$ we have that the corresponding density distributions satisfy $\rho' \neq \rho$. By the uniqueness of f once $\mathcal{V}$ is given, established above, it will be

sufficient to prove that there is a one to one correspondence between density distributions ρ and external potentials $\mathcal{V}$. In other words, $\mathcal{V}$ is completely determined by ρ. Only one external potential $\mathcal{V}$ is consistent with a given ρ.

In order to establish this, we will assume that there exist two external potentials $\mathcal{V}' \neq \mathcal{V}$ that give rise to exactly the same equilibrium density profile $\rho(\mathbf{r}_i)$ and deduct a contradiction. Since the external potentials differ, by the discussion above we know that their respective distribution functions f and f' must be different as well. We will distinguish between the primed and unprimed Hamiltonians

$$H' = K + \Phi + \mathcal{V}', \quad H = K + \Phi + \mathcal{V}. \tag{2.18}$$

Observing that we are still within the right setting for the Gibbs inequality to hold we see

$$\begin{aligned} \Omega[f_0'] &= \mathrm{Tr}_{cl} f_0'(H' - \mu N + \beta^{-1} \ln f_0') \\ &\leq \mathrm{Tr}_{cl} f_0(H' - \mu N + \beta^{-1} \ln f_0) \\ &= \Omega[f_0] + \mathrm{Tr}_{cl} f_0(H' - \mu N + \beta^{-1} \ln f_0) \\ &= \Omega[f_0] + \mathrm{Tr}_{cl} f_0(\mathcal{V}' - \mathcal{V}). \end{aligned} \tag{2.19}$$

However, since we assume both distributions to give rise to exactly the same density profile Eq. (2.19) is also valid upon interchanging primed and unprimed quantities. In combination with the following identity

$$\mathrm{Tr}_{cl}[f\mathcal{V}] = \mathrm{Tr}_{cl}\left(f\left(\int \sum_{i=1}^{N} V_{ext}(\mathbf{r})\delta(\mathbf{r} - \mathbf{r}_i) d\mathbf{r}\right)\right) = \int \rho(\mathbf{r}) V_{ext}(\mathbf{r}) d\mathbf{r}, \tag{2.20}$$

we arrive at the following inequality

$$\begin{aligned} \Omega[f_0] + \Omega[f_0'] < \Omega[f_0] + \Omega[f_0'] &+ \int \rho_0(\mathbf{r}) \left(V_{ext}'(\mathbf{r}) - V_{ext}(\mathbf{r})\right) d\mathbf{r} \\ &+ \int \rho_0(\mathbf{r}) \left(V_{ext}(\mathbf{r}) - V_{ext}'(\mathbf{r})\right) d\mathbf{r} \\ &= \Omega[f_0] + \Omega[f_0']. \end{aligned} \tag{2.21}$$

This clearly is a contradiction. Hence, our original assumption was wrong and we find that different external potentials give rise to different equilibrium density distributions, implying that f indeed is a functional of the density. □

2.1.3 Some variational calculus

For a moment it will look like we are introducing Ω as a functional of yet another function, but as it will turn out everything will come together nicely in the end. For now, we introduce the so called *local chemical potential* $u(\mathbf{r}) \equiv \mu - V_{ext}(\mathbf{r})$ and consider Ω to be a functional of this quantity. We can write $H_N - \mu N = K + \Phi - U$ where $U \equiv \sum_{i=1}^{N} u(\mathbf{r}_i)$. Considering the change in the grand potential upon a variation of $u(\mathbf{r})$ we find

$$
\begin{aligned}
\delta\Omega &= \Omega[u(\mathbf{r}+\delta u(\mathbf{r}_0)] - \Omega[u(\mathbf{r})] \\
&= -kT \ln \frac{\Xi[u(\mathbf{r})+\delta u(\mathbf{r})]}{\Xi[u(\mathbf{r})]} \\
&= -kT \ln \frac{\mathrm{Tr}_{cl} \exp[-\beta(H_N - \mu N - \delta U)]}{\mathrm{Tr}_{cl} \exp[-\beta(H_N - \mu N)]} \\
&= -kT \ln \frac{\mathrm{Tr}_{cl} \exp[-\beta(H_N - \mu N)](1+\beta\delta U)}{\Xi} \\
&= -kT \ln \left(1 + \beta\langle \delta U \rangle\right) \\
&= -\langle \delta U \rangle \\
&= -\mathrm{Tr}_{cl} f_0 \left(\delta \left(\sum_{i=1}^{N} \mu - V_{ext}(\mathbf{r_i}) \right) \right) \\
&= -\mathrm{Tr}_{cl} f_0 \left(\int \sum_{i=1}^{N} [\delta\mu - \delta V_{ext}(\mathbf{r}_i)] \delta(\mathbf{r}-\mathbf{r}_i) \right) \\
&= -\int d\mathbf{r} \rho_0(\mathbf{r}) \delta u(\mathbf{r}),
\end{aligned}
\tag{2.22}
$$

where we have used that the variation in U is small in order to use a generalized Taylor expansion around the argument of the logarithm up to first order. Now invoking the definition of the variational derivative, it is readily seen that we can rewrite above Eq. (2.22) in the following way

$$
\frac{\delta\Omega[u(\mathbf{r})]}{\delta u(\mathbf{r})} = -\rho_0(\mathbf{r}). \tag{2.23}
$$

The fact that the functional derivative of the grand potential with respect to the intrinsic chemical potential yields the negative equilibrium density allows for a generalized Legendre transformation of Ω with purpose of changing the function $u(\mathbf{r})$ by $\rho_0(\mathbf{r})$. This gives a functional that is known as the *intrinsic Helmholtz free energy functional*, $\mathcal{F}[\rho_0(\mathbf{r})]$, defined as

$$
\mathcal{F}[\rho_0(\mathbf{r})] = \Omega[u(\mathbf{r})] + \int d\mathbf{r} \rho_0(\mathbf{r}) u(\mathbf{r}). \tag{2.24}
$$

We can also functionally differentiate this new functional to its argument yielding

$$
\frac{\delta\mathcal{F}[\rho(\mathbf{r})]}{\delta\rho(\mathbf{r})} = \int d\mathbf{r}' \frac{\delta\Omega[u(\mathbf{r})]}{\delta u(\mathbf{r}')} \frac{\delta u(\mathbf{r}')}{\delta\rho(\mathbf{r})} + u(\mathbf{r}) + \int d\mathbf{r}' \frac{\delta u(\mathbf{r}')}{\delta\rho(\mathbf{r})} \rho(\mathbf{r}') = u(\mathbf{r}), \tag{2.25}
$$

where we have used the generalized version of the product rule and Eq. (2.23). This is the expected result and needed in order to do an inverse transformation, going back to the grand potential functional.

We consider now the explicit form of the grand potential as a functional of the density

$$
\Omega[\rho(\mathbf{r})] = \mathcal{F}[\rho(\mathbf{r})] - \int d\mathbf{r} \rho(\mathbf{r}) u(\mathbf{r}). \tag{2.26}
$$

Making use of the definition of $u(\mathbf{r})$, we write this as

$$\Omega[\rho(\mathbf{r})] = \mathcal{F}[\rho(\mathbf{r})] - \int d\mathbf{r}\rho(\mathbf{r})\left(V_{ext}(\mathbf{r}) - \mu\right), \tag{2.27}$$

which we consider at fixed μ and $\mathcal{V}$. It is now readily observed that $\rho_0(\mathbf{r})$ is an extremum of the functional (2.27)

$$\frac{\delta\Omega[\rho(\mathbf{r})]}{\delta\rho(\mathbf{r})}\Big|_{\rho(\mathbf{r})=\rho_0(\mathbf{r})} = \frac{\delta\mathcal{F}[\rho(\mathbf{r})]}{\delta\rho(\mathbf{r})}\Big|_{\rho(\mathbf{r})=\rho_0(\mathbf{r})} + V_{ext}(\mathbf{r}) - \mu = u(\mathbf{r}) - u(\mathbf{r}) = 0. \tag{2.28}$$

2.1.4 Putting things together

Equation (2.28) provides an explicit way for calculating the equilibrium density profile when $\mathcal{F}[\rho(\mathbf{r})]$ is known. At this point we have established a lot of claims, and now it is time to put them all together. We have managed to show that $\Omega[\rho(\mathbf{r})]$ is extremized at the equilibrium density distribution, but not that this is a minimum. Nor have we showed that this functional is actually unique. So it is time to make the connection to the theorems that we have proved in the earlier section of this chapter.

In Eq. (2.19) we have established that the equilibrium distribution f_0 is a unique functional of the equilibrium density ρ_0. From this it is readily seen that Eq. (2.24) is a unique functional of the density

$$\begin{aligned}
\mathcal{F}[\rho_0] &= \mathrm{Tr}_{cl} f_0\left(K + \Phi + kT\ln f_0\right) \\
&= \mathrm{Tr}_{cl} f_0\left(K + \Phi - U + U + kT\ln f_0\right) \\
&= \Omega[u] + \mathrm{Tr}_{cl}\left(\int \sum_{i=1}^{N} u(\mathbf{r})\delta(\mathbf{r} - \mathbf{r}_i)\right) \\
&= \Omega[u] + \int d\mathbf{r}\rho_0(\mathbf{r})u(\mathbf{r}).
\end{aligned} \tag{2.29}$$

This form is valid for *all* external potentials and chemical potentials. This fact makes this functional extremely useful for making educated guesses for further applications.

We now turn our attention to the grand potential functional Eq.(2.27),

$$\begin{aligned}
\Omega[\rho(\mathbf{r})] &= \mathcal{F}[\rho] - \int d\mathbf{r}\rho(\mathbf{r})\left(V_{ext}(\mathbf{r}) - \mu\right) \\
&= Tr_{cl}\left(K + \Phi + kT\ln f + \mathcal{V} - \mu N\right) \\
&= Tr_{cl}\left(H_N - \mu N + kT\ln f\right) \\
&= \Omega[f].
\end{aligned} \tag{2.30}$$

And thus we can use the Gibbs inequality once more we can conclude that the equilibrium density profile ρ_0 does in fact minimize the grand potential functional Ω

$$\Omega[\rho_0] < \Omega[\rho], \forall\rho(\mathbf{r}) \neq \rho_0(\mathbf{r}). \tag{2.31}$$

The above functionals are the pillars on which applications of density functional theory rests. We can now summarize all of the above in the so called fundamental equations of nonuniform fluids

$$\frac{\delta\Omega[\rho(\mathbf{r})]}{\delta\rho(\mathbf{r})}\Big|_{\rho_0(\mathbf{r})} = 0, \quad \Omega[\rho_0] = \Omega, \tag{2.32}$$

and

$$\frac{\delta\mathcal{F}[\rho(\mathbf{r})]}{\delta\rho(\mathbf{r})}\Big|_{\rho_0(\mathbf{r})} = \mu - V_{ext}(\mathbf{r}). \tag{2.33}$$

From thermodynamics we know that the Helmholtz free energy of a system is given by $F = \Omega + \mu N$. Using that $N = \int d\mathbf{r}\rho_0(\mathbf{r})$ we obtain

$$F = \mathcal{F}[\rho_0] + \int d\mathbf{r}\rho_0(\mathbf{r})V_{ext}(\mathbf{r}). \tag{2.34}$$

Thus, by functional minimization of the grand potential functional one obtains the thermodynamic properties of the system through the grand potential Ω and the structure of the system through the density profile $\rho_0(\mathbf{r})$.

2.1.5 The ideal-gas free energy functional

In statistical physics an ideal gas is a system of particles where there is no inter-particle interaction. Such a system is characterized by the following Hamiltonian

$$H_{id} = K + \mathcal{V}. \tag{2.35}$$

It turns out that in this case it is possible to calculate the Helmholtz functional exactly. First we write out the grand canonical partition function for this system in its full generality,

$$\begin{aligned}
\Xi_{id} &= \sum_{N=0}^{\infty} \frac{1}{N!h^{3N}} \int \exp[\beta(\mu N - \sum_{i=1}^{N} \frac{\mathbf{p}_i{}^2}{2m} - \sum_{i=1}^{N} V_{ext}(\mathbf{r}_i))] d\mathbf{p}_1 \cdots d\mathbf{p}_N d\mathbf{r}_1 \cdots d\mathbf{r}_N \\
&= \sum_{N=0}^{\infty} \frac{1}{N!\Lambda^{3N}} \int \exp[\beta(\mu N - \sum_{i=1}^{N} V_{ext}(\mathbf{r}_i))] d\mathbf{r}_1 \cdots d\mathbf{r}_N \\
&= \sum_{N=0}^{\infty} \frac{1}{N!\Lambda^{3N}} \int \exp[\beta(\sum_{i=1}^{N} \delta(\mathbf{r} - \mathbf{r}_i)u(\mathbf{r}))] d\mathbf{r}_1 \cdots d\mathbf{r}_N \\
&= \sum_{N=0}^{\infty} \frac{1}{N!\Lambda^{3N}} \left(\int d\mathbf{r} \exp[\beta u(\mathbf{r})] \right)^N \\
&= \exp[\Lambda^{-3} \int d\mathbf{r} \exp[\beta u(\mathbf{r})]]
\end{aligned} \tag{2.36}$$

where we have used the power series expansion of $\exp(x)$ and introduced the thermal (De Broglie) wavelength $\Lambda \equiv \frac{h}{\sqrt{2\pi m k_b T}}$. Now using the definition of the Helmholtz free energy functional Eq. (2.24) we can write

$$\begin{aligned}\mathcal{F}[\rho(\mathbf{r})] &= \Omega[u(\mathbf{r})] + \int d\mathbf{r}\rho(\mathbf{r})u(\mathbf{r})) \\ &= -kT\ln[\Xi_{id}] + \int d\mathbf{r}\rho(\mathbf{r})u(\mathbf{r})) \\ &= -\Lambda^{-3}\int d\mathbf{r}\exp[u(\mathbf{r})] + \int d\mathbf{r}\rho(\mathbf{r})u(\mathbf{r})).\end{aligned} \tag{2.37}$$

Invoking the relation between the density $\rho(\mathbf{r})$ and the intrinsic chemical potential $u(\mathbf{r})$, that one can find by functional differentation of $\Omega[u(\mathbf{r})]$, Eq. (2.23), we find the following result

$$\mathcal{F}_{id}[\rho(\mathbf{r}] = kT\int d\mathbf{r}\rho(\mathbf{r})\left(\ln\rho(\mathbf{r})\Lambda^3 - 1\right). \tag{2.38}$$

This is useful because for a generic inter-particle interaction it is possible to split the intrinsic free energy functional into two parts, an *ideal* and an *excess* part,

$$\mathcal{F} = \mathcal{F}_{id} + \mathcal{F}_{ex}. \tag{2.39}$$

The second part, the over-deal gas free energy functional, contains all the information regarding interparticle interactions. The variational principle developed in the section above now takes the following form

$$\begin{aligned}\frac{\delta\Omega[\rho(\mathbf{r})]}{\delta\rho(\mathbf{r})} &= 0 \\ &= \frac{\delta\mathcal{F}[\rho(\mathbf{r})]}{\delta\rho(\mathbf{r})} + V_{ext}(\mathbf{r}) - \mu \\ &= \frac{\delta\mathcal{F}_{id}[\rho(\mathbf{r})]}{\delta\rho(\mathbf{r})} + \frac{\delta\mathcal{F}_{ex}[\rho(\mathbf{r})]}{\delta\rho(\mathbf{r})} + V_{ext}(\mathbf{r}) - \mu \\ &= kT\ln\Lambda^3\rho(\mathbf{r}) + \frac{\delta\mathcal{F}_{ex}[\rho(\mathbf{r})]}{\delta\rho(\mathbf{r})} + V_{ext}(\mathbf{r}) + \mu.\end{aligned} \tag{2.40}$$

Additionally we can split the total chemical potential μ into an ideal gas contribution μ_{id} and an excess contribution μ_{ex} where $\mu_{id} = kT\ln\Lambda^3\rho_{bulk}$, where we have introduced ρ_{bulk} as the constant density of the bulk fluid in consideration. Introducing the *one body correlation function*

$$c^{(1)}(\mathbf{r}) = -kT\frac{\delta\mathcal{F}_{ex}[\rho(\mathbf{r})]}{\delta\rho(\mathbf{r})}, \tag{2.41}$$

we can write Eq.(2.40) in the following self-consistent form

$$\rho(\mathbf{r}) = \rho_{bulk}\exp[-\beta V_{ext}(\mathbf{r}) + c^{(1)}(\mathbf{r}) + \beta\mu_{ex}]. \tag{2.42}$$

2.2 Generalization to multicomponent mixtures

So far we have only taken into consideration mixtures of one type of particle. The generalization to systems consisting of more particles is a quite straightforward generalization of the theory developed above. For this reason we will not go through the entire derivation, but we will just state the results. These will be needed later on when we are considering two species of oppositely charged particles. For the general case, suppose that we have ν different particle species. In this case the relevant functionals depend on all $\{\rho_i\}, i \in \{1 \cdots \nu\}$ density profiles for the particular species. The grand potential functional in this case becomes

$$\Omega[\{\rho_i\}] = \sum_{i=1}^{\nu} k_b T \int d\mathbf{r} \rho_i(\mathbf{r}) \left(\ln \Lambda_i^3 \rho_i(\mathbf{r}) - 1 \right) + \mathcal{F}_{ex}[\{\rho_i\}] + \sum_{i=1}^{\nu} \int d\mathbf{r} \rho_i(\mathbf{r}) \left(V_{ext}^i(\mathbf{r}) - \mu_i \right), \tag{2.43}$$

where Λ_i is the thermal wavelength of species i. The unspecified excess free energy functional depends on the density profiles $\{\rho_i(\mathbf{r})\}$ of all species. Minimizing the grand potential functional amounts to solving the system of coupled equations

$$\frac{\delta \Omega[\{\rho_i\}]}{\delta \rho_i}\Big|_{\rho_j = \rho_0^j} = 0, \quad i \in \{1 \cdots \nu\}. \tag{2.44}$$

2.3 The derivatives of the free energy functional, towards Ornstein-Zernike

Adding an inter-particle interaction term to the Hamiltonian drastically increases the complexity of statistical physics problem. When this is the case we in generally cannot make use of nice factorization properties of the exponents, and it will in most cases be impossible to find the free energy functional by using Eq. (2.29). In this section we will use certain properties of the functional derivatives of $\mathcal{F}$ in order to approximate $\mathcal{F}$ itself.

We introduce now the n-body direct correlation function $c^{(n)}$

$$c^{(n)}(\mathbf{r}_1 \cdots \mathbf{r}_n; [\rho]) = -\beta \frac{\delta^n \mathcal{F}_{ex}[\rho]}{\delta \rho(\mathbf{r}_1) \cdots \delta \rho(\mathbf{r}_n)}. \tag{2.45}$$

From its definition we see that $c^{(n)}$ is symmetric under the permutation of its arguments $\mathbf{r}_i$ and that for $n \geq 1$

$$c^{(n)}(\mathbf{r}_1 \cdots \mathbf{r}_{n+1}; [\rho]) = \frac{c^{(n)}(\mathbf{r}_1 \cdots \mathbf{r}_n; [\rho])}{\delta \rho(\mathbf{r}_{n+1})}. \tag{2.46}$$

Plugging $\mathcal{F} = \mathcal{F}_{id} + \mathcal{F}_{ex}$ in the fundamental equation Eq. (2.33) we obtain the following identity

$$\ln \rho_0(\mathbf{r}) \Lambda^3 - c^{(1)}(\mathbf{r}; [\rho_0]) = \beta u(\mathbf{r}). \tag{2.47}$$

We can now consider the functional derivative of Eq. (2.47) with respect to $\rho_0(\mathbf{r}')$. Doing this we obtain the identity

$$\frac{1}{\rho_0(\mathbf{r})}\delta(\mathbf{r}-\mathbf{r}') - c^{(2)}(\mathbf{r},\mathbf{r}';[\rho_0]) = \beta\frac{\delta u(\mathbf{r})}{\delta\rho_0(\mathbf{r}')}. \tag{2.48}$$

We will prove the following lemma regarding this equation

Lemma 2.3.1. *The right hand side of equation (2.48) is invertible and given explicitely by*

$$\frac{1}{\beta}\frac{\delta\rho_0(\mathbf{r})}{\delta u(\mathbf{r}')} = \rho_0(\mathbf{r})\rho_0(\mathbf{r}')h(\mathbf{r},\mathbf{r}') + \rho_0(\mathbf{r})\delta(\mathbf{r},\mathbf{r}'), \tag{2.49}$$

where $h(\mathbf{r},\mathbf{r}') = g(\mathbf{r},\mathbf{r}') - 1$ is the total correlation function, defined by means of the two-body density

$$\rho^{(2)}(\mathbf{r},\mathbf{r}') = \langle\sum_{i\neq j}^{N}\delta(\mathbf{r}-\mathbf{r}_i)\delta(\mathbf{r}-\mathbf{r}_j)\rangle \equiv \widehat{\rho}_0(\mathbf{r})\widehat{\rho}_0(\mathbf{r}')g(\mathbf{r},\mathbf{r}') \tag{2.50}$$

Proof. We start by writing the grand partition function as a functional of the intrinsic local chemical potential $u(\mathbf{r})$

$$\begin{aligned}\Xi &= \sum_{N=0}^{\infty}\frac{\exp[\beta\mu N]}{N!\Lambda^{3N}}\int d^N\mathbf{r}\exp[-\beta\Phi(\mathbf{r}^N) - \beta\sum_{i=1}^{N}V_{ext}(\mathbf{r}_i)] \\ &= \sum_{N=0}^{\infty}\frac{\exp[\beta\mu N]}{N!\Lambda^{3N}}\int d^N\mathbf{r}\exp[-\beta\Phi(\mathbf{r}^N) + \beta\int d\mathbf{r}u(\mathbf{r})\rho(\mathbf{r})].\end{aligned} \tag{2.51}$$

Straightforward, repetitive functional differentation with respect to $u(\mathbf{r})$ yields

$$\frac{1}{\beta\Xi}\frac{\delta\Xi}{\delta u(\mathbf{r})} = \langle\widehat{\rho}(\mathbf{r})\rangle = \rho_0(\mathbf{r}), \tag{2.52}$$

$$\frac{1}{\beta^2\Xi}\frac{\delta^2\Xi}{\delta u(\mathbf{r})\delta u(\mathbf{r}')} = \langle\widehat{\rho}(\mathbf{r})\widehat{\rho}(\mathbf{r}')\rangle = \rho^{(2)}(\mathbf{r},\mathbf{r}') + \rho_0(\mathbf{r})\delta(\mathbf{r}-\mathbf{r}'). \tag{2.53}$$

Combining all this yields the desired result

$$\begin{aligned}\frac{\delta\rho_0(\mathbf{r})}{\delta\beta u(\mathbf{r}')} &= \frac{\delta}{\delta\beta u(\mathbf{r}')}\frac{1}{\Xi}\frac{\delta\Xi}{\delta\beta u(\mathbf{r})} \\ &= \frac{1}{\Xi}\frac{\delta^2\Xi[u]}{\delta\beta u(\mathbf{r})\delta\beta u(\mathbf{r}')} - \frac{1}{\Xi^2}\frac{\delta\Xi[u]}{\delta\beta u(\mathbf{r})}\frac{\delta\Xi[u]}{\delta\beta u(\mathbf{r}')} \\ &= \langle\rho(\mathbf{r})\rho(\mathbf{r}')\rangle - \rho_0(\mathbf{r})\rho_0(\mathbf{r}') \\ &= \rho^{(2)}(\mathbf{r},\mathbf{r}') - \rho_0(\mathbf{r})\rho_0(\mathbf{r}') + \rho_0(\mathbf{r})\delta(\mathbf{r},\mathbf{r}') \\ &= \rho_0(\mathbf{r})\rho_0(\mathbf{r}')h(\mathbf{r},\mathbf{r}') + \rho_0(\mathbf{r})\delta(\mathbf{r},\mathbf{r}')\end{aligned} \tag{2.54}$$

□

Together with the identity

$$\int d\mathbf{r}'' \frac{\delta\beta u(\mathbf{r})}{\delta\rho_0(\mathbf{r}'')} \frac{\delta\rho_0(\mathbf{r}'')}{\delta\beta u(\mathbf{r}')} = \delta(\mathbf{r}-\mathbf{r}'), \tag{2.55}$$

we find that

$$h(\mathbf{r},\mathbf{r}') = c^{(2)}(\mathbf{r},\mathbf{r}') + \int d\mathbf{r}'' c^{(2)}(\mathbf{r},\mathbf{r}'')\rho_0(\mathbf{r}'')h(\mathbf{r}'',\mathbf{r}'). \tag{2.56}$$

Above Eq. (2.56) is called the Ornstein-Zernike equation. Together with an independent second equation, known as the closure, connecting the total correlation function h and the direct correlation function c can be used to solve the OZ-equation.

2.3.1 An example, the virial expansion and the Mayer-function

It is relatively straightforward to perform a low density expansion around the ideal gas for homogeneous fluids [5]. This so called virial expansion for the case of inhomogeneous fluids yields

$$\mathcal{F}[\rho] = \mathcal{F}_{id}[\rho] - \frac{kT}{2}\int d\mathbf{r}d\mathbf{r}' f(\mathbf{r},\mathbf{r}')\rho(\mathbf{r})\rho(\mathbf{r}'). \tag{2.57}$$

Where we have introduced the Mayer-function

$$f(\mathbf{r},\mathbf{r}') = \exp[\beta\phi(|\mathbf{r}-\mathbf{r}'|)] - 1. \tag{2.58}$$

We immediately see that this functional depends on the interparticle interaction, but not on the external potential or the chemical potential, as predicted by the general framework. By means of the fundamental equation of inhomogeneous fluids we arrive at the following expression for the equilibrium density profile

$$\rho_0(\mathbf{r}) = z\exp[-\beta V_{ext}(\mathbf{r}) + \int d\mathbf{r}' f(\mathbf{r},\mathbf{r}')\rho_0(\mathbf{r}')], \tag{2.59}$$

which is an implicit equation for the density profile, being that ρ appears on both sides of the equation. This equation can by solved by numerical methods, e.g. a Picard iteration which we will come back to later.

Chapter 3

Lennard-Jones Functionals

Calculating the excess free energy functional is in general not possible exactly. In some cases there are approximations that are quite good. In 1989 Rosenfeld proposed a way to derive a DFT functional for mixtures of hard-sphere particles [13]. His method is based on some of the fundamental geometric properties of spheres. The starting point of Rosenfelds hard-sphere functional is the exactly known functional for hard rods in one dimension. Later on the Rosenfeld FMT was improved by Tarazona [14]. After that multiple additional improvements have been made. In this chapter we will decompose the excess free energy functional for Lennard-Jones fluids into a repulsive and an attractive part. We will look at Rosenfelds original development and state the extension that is used in the numerical code for the hard sphere part. The attractive part is of a mean field form and the result will be stated here. This chapter follows the introduction of FMT of [7]

3.1 Hard Rods in One Dimension: an Exact Result

Besides the ideal gas model, there are no continuous models for which the statistical physics can be solved analytically in three dimensions. In one dimension however such models do exist. It turns out that for rod-like particles in one dimension, the free energy functional $\mathcal{F}$ can be calculated exactly. This result is the starting point of Rosenbergs fundamental measure theory. Robledo and Varea derived the following grand potential functional for this system [16]

$$\Omega[\rho(z)] = \mathcal{F}_{id} + \mathcal{F}_{ex} - \int dz\mu - V_{ext}(z)\rho(z). \tag{3.1}$$

They managed to exactly find the excess free energy functional

$$\mathcal{F}_{ex} = \beta^{-1} \int dz\rho(z)\ln[1 - t(z)], \tag{3.2}$$

with $t(z) = \int_{z-\sigma}^{z} dz'$ with σ the lenght of the rods. Extremezing Eq. (3.1) yields the following equation

$$\beta u(z) = \ln \frac{\Lambda\rho(z)}{1 - t(z)} + \int_{z}^{z+\sigma} dy \frac{\rho(y)}{1 - t(y)}. \tag{3.3}$$

They extended this to mixtures of different lengths $2R_j$, showing that the excess free energy functional in this case takes the form

$$\beta\mathcal{F}_{ex}[\{\rho_i\}] = \int dz \Phi_{ex}\left(\{n_\alpha(z)\}\right), \tag{3.4}$$

where the $\{\rho_i\}$ are the density profiles of the rods with respective length $2R_i$. Φ_{ex} is the excess free energy density as a function of a set of weighted densities n_α, defined as

$$n_\alpha(z) = \sum_{i=1}^{\mu} \int dz' \rho_i(z') w_i^\alpha(z - z'). \tag{3.5}$$

That is, the weight functions are sums of the density of species i with a weight function that is characteristic for species i, determined by the specific geometry of the species. In the one dimensional case there are two different weight functions, associated with the surface of the rod and the volume of the rod, respectively

$$w_i^{(0)}(z) = \frac{1}{2}\left(\delta(z + R_i) + \delta(z - R_i),\right) \tag{3.6}$$

and

$$w_i^{(1)}(z) = \Theta(R_i - |z|), \tag{3.7}$$

where the Heaviside step function is defined as

$$\Theta(x) = \begin{cases} 1 & x > 0 \\ 0 & x \leq 0 \end{cases} \tag{3.8}$$

The free energy density takes the following form

$$\Phi_{ex}(n_\alpha) = -n_0 \ln(1 - n_1). \tag{3.9}$$

In the theory of simple liquids the Mayer function plays an important role. See e.g.[5]. The Mayer function, commonly denoted with f, is given by

$$f_{ij}(z) = \exp[\beta\phi_{ij}(z)] - 1. \tag{3.10}$$

Using the hard rod potential they Mayer function can take on the following values

$$f_{ij} = \begin{cases} -1 & |z| < R_i + R_j \\ 0 & \text{otherwise} \end{cases} \tag{3.11}$$

Fundamental measure theory is based on the fact that the Mayer function Eq. (3.10) can be written as convolutions of suitable weight functions. Denoting the convolution with $\otimes$

$$w_i^{(\alpha)} \otimes w_j^{(\beta)} = \int dz' w_i^{(\alpha)}(z' - z_i) w_j^{(\beta)}(z_j - z'), \tag{3.12}$$

it turns out that the one dimensional Mayer function can be written as

$$-f_{ij}(z) = w_1^{(i)} \otimes w_0^{(j)} + w_0^{(i)} \otimes w_1^{(j)}. \tag{3.13}$$

3.2 Rosenfelds three dimensional FMT

Rosenfelds goal was to find the explicit form of the free energy functional for a mixture of ν species of hard spheres in three dimensions with radii R_i. His starting point was the exact solution for a system of one dimensional hard rods, as developed above. He extended this to in three dimensions, assuming a low-density limit for every species. The low density excess free energy functional in this three dimensional case looks like

$$\beta\mathcal{F}_{ex} = -\frac{1}{2}\sum_{i,j}\int d\mathbf{r}\int d\mathbf{r}'\rho_i(\mathbf{r})\rho_j(\mathbf{r}')f_{ij}(|\mathbf{r}-\mathbf{r}'|). \tag{3.14}$$

He cleverly wrote the three dimensional Mayer function f_{ij} as a sum of particular convolutions of weight functions. Here ϕ denotes the three dimensional hard-sphere potential Eq. (C.7) and r_{ij} is the separation distance between particle i, j. This results in the following possible values of f

$$f_{ij}(r_{ij}) = \begin{cases} -1 & |r_{ij}| < R_i + R_j \\ 0 & \text{otherwise} \end{cases} \tag{3.15}$$

Rosenfeld showed that the Mayer function can be decomposed in terms of weighted densities as

$$-f_{ij} = w_3^{(i)}\otimes w_0^{(j)} + w_0^{(i)}\otimes w_3^{(j)} + w_2^{(i)}\otimes w_1^{(j)} + w_1^{(i)}\otimes w_2^{(j)} - \vec{w}_2^{(i)}\otimes\vec{w}_1^{(j)} - \vec{w}_1^{(i)}\otimes\vec{w}_2^{(j)} \tag{3.16}$$

Where $\otimes$ now denotes the three dimensional convolution

$$w_i^{(\alpha)}(\mathbf{r_i})\otimes w_j^{(\beta)}(\mathbf{r_j}) = \int d\mathbf{r}' w_i^{(\alpha)}(\mathbf{r}'-\mathbf{r}_i)w_j^{(\beta)}(\mathbf{r}'-\mathbf{r}_j) \tag{3.17}$$

where the weight functions are given by

$$\begin{aligned} w_3^{(i)}(\mathbf{r}) &= \Theta(R_i - r), & w_2^{(i)}(\mathbf{r}) &= \delta(R_i - r), \\ w_1^{(i)}(\mathbf{r}) &= \frac{w_2^{(i)}(\mathbf{r})}{4\pi R_i}, & w_0^{(i)}(\mathbf{r}) &= \frac{w_2^{(i)}(\mathbf{r})}{4\pi R_i^2}, \\ \vec{w}_2^{(i)}(\mathbf{r}) &= \frac{\mathbf{r}}{r}\delta(R_i - r), & \vec{w}_1^{(i)}(\mathbf{r}) &= \frac{\vec{w}_2^{(i)}(\mathbf{r})}{4\pi R_i}. \end{aligned} \tag{3.18}$$

Analogously to the one dimensional case, the convolution of weight function gives rise to a set of weighted densities $\{n_\alpha(\mathbf{r})\}$ that are the sum of convolutions of the density profile of each specie with a weight function

$$n_\alpha(\mathbf{r}) = \sum_{i=1}^{\nu}\int d\mathbf{r}'\rho_i(\mathbf{r}')w_\alpha^{(i)}(\mathbf{r}-\mathbf{r}'). \tag{3.19}$$

Again in analogy with the exact one dimensional case, Rosenfeld made the following ansatz for the excess free energy functional of the hard sphere mixture

$$\beta\mathcal{F}_{ex} = \int d\mathbf{r}'\Phi\left(\{n_\alpha(\mathbf{r}')\}\right), \tag{3.20}$$

where the energy density Φ is again a function of the weighted densities of all species. Rosenfeld wrote for Φ the expression (for this ansatz he used a technique known as dimensional analysis)

$$\Phi = f_1(n_3)n_0 + f_2(n_3)n_1n_2 + f_3(n_3)\vec{n_1}\cdot\vec{n_2} + f_4(n_3)n_2^2 + f_5(n_3)n_2\vec{n_2}\cdot\vec{n_3}. \tag{3.21}$$

In ensuring the right deconvolution of the Mayer function it turns out that we need the unknown functions f_1, f_2, f_3 to lowest order in n_3

$$\begin{aligned} f_1 &= n_3 + \mathcal{O}(n_3^2) \\ f_2 &= 1 + \mathcal{O}(n_3^2) \\ f_3 &= -1 + \mathcal{O}(n_3^2) \\ f_4 &= \frac{1}{24}\pi + \mathcal{O}(n_3^2) \\ f_5 &= -\frac{3}{24}\pi + \mathcal{O}(n_3^2). \end{aligned} \tag{3.22}$$

This ansatz produces an exact result in the low density limit. For higher densities this ansatz incorporates the approximations that the weight functions and thus also the weighted densities are sufficient to incorporate the simultaneous interaction of three hard spheres.

Given a suitable thermodynamic condition the unknown functions f_1, f_2, f_3, f_4, f_5 can be determined. In the original paper by Rosenfeld [13] the so called SPT condition was used

$$\lim_{R_i\to\infty} \frac{\mu_{ex}^i}{V_i} = p, \tag{3.23}$$

with μ_{ex}^i denoting the excess chemical potential of species i and $V_i = \frac{4\pi R_i^3}{3}$ the volume of a spherical particle of species i. We can express the left hand side of this equation in terms of weighted densities in the following manner

$$\beta\mu_{ex}^i = \frac{\partial\Phi}{\partial\rho_i} = \sum_\alpha \frac{\partial\Phi}{\partial n_\alpha}\frac{\partial n_\alpha}{\partial\rho_i}. \tag{3.24}$$

Since the weight functions are determined by geometry, it can be shown that the derivatives with respect to the densities are

$$\frac{\partial n_3}{\partial\rho_i} = V_i, \quad \frac{\partial n_2}{\partial\rho_i} = 4\pi R_i^2, \quad \frac{\partial n_1}{\partial\rho_i} = R_i, \quad \frac{\partial n_0}{\partial\rho_i} = 1. \tag{3.25}$$

Considering the above limit we are left with

$$\lim_{R_i\to\infty} \frac{\mu_{ex}^i}{V_i}\beta = \frac{\partial\Phi}{\partial n_3}. \tag{3.26}$$

Using the equation of state and the expression for the bulk grand potential

$$\Omega_{bulk} = -pV, \;\; \Omega_{bulk}/V = \Phi + f_{id} - \sum_i \rho^i_{bulk}\mu^i, \tag{3.27}$$

we arrive at the differential equation

$$\frac{\partial \Phi}{\partial n_3} = -\Phi + \sum_\alpha \frac{\partial \Phi}{\partial n_\alpha} n_\alpha + n_0. \tag{3.28}$$

By collecting terms proportional to n_α you can obtain the differential equations for the f's. The integration constants are chosen such that the desired behaviour in the low density regime is obtained. Rosenfeld showed that they read

$$\begin{aligned} f_1(n_3) &= -\ln(1-n_3) \\ f_2(n_3) &= \frac{1}{1-n_3} \\ f_3(n_3) &= -f_2(n_3) \\ f_4(n_3) &= \frac{1}{24\pi(1-n_3)^2} \\ f_5(n_3) &= -3f_4(n_3). \end{aligned} \tag{3.29}$$

Now inserting these expressions back into Eq.(3.21) we find the Rosenfeld FMT functional. Often it is written in the decomposed way $\Phi = \Phi_1 + \Phi_2 + \Phi_3$ where

$$\Phi_1 = -n_0 \ln(1-n_3); \;\; \Phi_2 = \frac{n_1 n_2 - \vec{n_1}\cdot\vec{n_2}}{1-n_3}; \;\; \Phi_3 = \frac{n_2^2 - 3n_2\vec{n_2}\cdot n_2}{24\pi(1-n_3)^2}$$

3.3 Extension with tensor weight functions

An extension of the original FMT functional by Rosenfeld was introduced by Tarazona [14]. Since then many improvements have been made. For the readers convenience the full extension we will use, called the White Bear II FMT, is stated here. The excess free energy functional for hard sphere interactions is

$$\beta\mathcal{F}_{WB} = \int d\mathbf{r}\Phi^{WB}(\{n_\alpha(\mathbf{r}), \mathbf{v}_\alpha(\mathbf{r}), \mathbf{T}_\alpha(\mathbf{r})\}) \tag{3.30}$$

The density profiles are convolved with the kernels w_i^α, yielding the tensorial weight functions

$$n_\alpha(\mathbf{r}) = \sum_i \int d\mathbf{r}'\rho_i(\mathbf{r}) w_i^\alpha(\mathbf{r}-\mathbf{r}') \tag{3.31}$$

$$\mathbf{v}_\alpha(\mathbf{r}) = \sum_i \int d\mathbf{r}'\rho_i(\mathbf{r}) \vec{w}_i^\alpha(\mathbf{r}-\mathbf{r}') \tag{3.32}$$

$$\mathbf{T}_\alpha(\mathbf{r}) = \sum_i \int d\mathbf{r}'\rho_i(\mathbf{r}) \mathbf{w}_i^\alpha(\mathbf{r}-\mathbf{r}') \tag{3.33}$$

With the scalar, vector and tensor weight functions given by

$$\begin{aligned}
w_3^{(i)}(\mathbf{r}) &= \Theta(R_i - r) \\
w_2^{(i)}(\mathbf{r}) &= \delta(R_i - r) \\
w_1^{(i)}(\mathbf{r}) &= \frac{w_2^{(i)}(\mathbf{r})}{4\pi R_i} \\
w_0^{(i)}(\mathbf{r}) &= \frac{w_2^{(i)}(\mathbf{r})}{4\pi R_i^2} \\
\vec{w}_2^{(i)}(\mathbf{r}) &= \frac{\mathbf{r}}{r}\delta(R_i - r) \\
\vec{w}_1^{(i)}(\mathbf{r}) &= \frac{\vec{w}_2^{(i)}(\mathbf{r})}{4\pi R_i} \\
\mathbf{w}^{(2)}(\mathbf{r}) &= \left(\frac{\mathbf{r}\cdot\mathbf{r}^T}{|\mathbf{r}|^2} - \frac{I}{3}\right) w^{(2)}(\mathbf{r})
\end{aligned} \tag{3.34}$$

The expression for the White Bear free energy density reads

$$\begin{aligned}
\Phi^{WB} = -n_0\ln(1-n_3) &+ \left(1 + \frac{1}{9}n_3^2\Phi_2(n_3)\right)\frac{n_1 n_2 - \mathbf{v}_1\cdot\mathbf{v}_2}{1-n_3} \\
&+ \left(1 - \frac{4}{9}n_3\Phi_3(n_3)\right)\frac{n_2^3 - 3n_2\mathbf{v}_2\cdot\mathbf{v}_2 + \frac{9}{2}\left(\mathbf{v}_2^t\cdot\mathbf{T}_2\cdot\mathbf{v}_2 - Tr\left(\mathbf{T}_2^3\right)\right)}{24\pi(1-n_3)^2}
\end{aligned} \tag{3.35}$$

Where the functions Φ_2 and Φ_3 are given by

$$\Phi_2(n_3) = \frac{6n_3 - 3n_3^2 + 6(1-n_3)\ln(1-n_3)}{n_3^3}, \tag{3.36}$$

$$\Phi_3(n_3) = \frac{6n_3 - 9n_3^2 + 6n_3^3 + 6(1-n_3)^2\ln(1-n_3)}{4n_3^3}. \tag{3.37}$$

3.4 Attractive Lennard-Jones interactions

There are multiple ways to decompose the LJ-potential (C.5) in its repulsive and attractive part. Barker and Henderson showed the 12-6 Lennard-Jones can be separated in the following manner [15],

$$\phi_{LJ}(r) = \phi_{rep}(r) + \phi_{attr}(r), \tag{3.38}$$

with

$$\phi_{rep}(r) = \begin{cases} \phi_{LJ}(r) & r \le \sigma \\ 0 & \text{otherwise,} \end{cases} \tag{3.39}$$

and

$$\phi_{att}(r) = \begin{cases} 0 & r \leq \sigma \\ \phi_{LJ}(r) & \text{otherwise.} \end{cases} \tag{3.40}$$

Here σ is the distance at which the inter-particle interaction is zero and r is the separation distance between two particles. The ϕ_{rep} is based on a hard-sphere model with an effective hard-sphere diameter d, not always equal to σ.

For Lennard-Jones fluids the excess free energy functional is decomposed into a repulsive (HS) and an attractive (att) part,

$$\mathcal{F}_{LJ} = \mathcal{F}_{HS} + \mathcal{F}_{att}. \tag{3.41}$$

The repulsive part is approximated by a HS-functional with diameter d, in our case the WB II functional. The attractive part of Eq. (3.41) is now realized in a mean-field manner,

$$\mathcal{F}_{att} = \frac{1}{2} \int \int \rho(\mathbf{r}) \rho(\mathbf{r}') \phi_{attr}(|\mathbf{r} - \mathbf{r}'|) d\mathbf{r} d\mathbf{r}'. \tag{3.42}$$

Chapter 4

Electrostatic Functionals

In this chapter we will examine the Hamiltonian of a mixture of cations and anions dissolved in some medium with fixed dielectric constant ϵ. The interaction between ions and charged surfaces is of paramount importance in many areas of physics and chemistry. We will state a mean field functional incorporating these interactions and look at the predictions this functional makes for the ionic density profiles in the absence of other interactions. After that we will briefly discuss two functionals taking ionic correlations into consideration. These functionals will play an important role in predicting the structure of high density ionic liquids with asymmetric particles.

Since DFT is to be applied in the situation of ionic liquids in contact with planar electrodes another key ingredient for the development of the theory is the theory of electrostatics in liquids. The basic notions as well as the relationship to DFT will be introduced in this chapter. The topics discussed and the development of these topics closely follow [5].

The dielectric constant ϵ, or also commonly referred to as the (relative) permittivity, is a measure for the decrease in force between charged entities as compared to vacuum. The larger the dielectric constant of a medium, the larger *decrease* of force between charged entities in that medium at the same distance as compared to vacuum. Since the dielectric constant of water is a whole lot greater than air, $\frac{\epsilon_{\text{water}}}{\epsilon_{\text{air}}} \simeq 80$ the energetic cost of separating neutral molecules in charged constituents is far less in water than air. From thermodynamics we know that systems at fixed temperature T strive to minimize their free energy $F = U - TS$. The fact that the increase in U when doing work against the Coulombic interaction of oppositely charged ions is much less in water than in air combined with entropic gain when dissociating some neutral element into multiple charged constituents makes that one often sees free ions in water that one would not observe in air (the most basic example being the immediate dissociation of NaCl in water). But this is not the only thing the large dielectric constant of water is responsible for. It is also responsible for a dissociation tendency of chemical groups residing on the surface of any object placed in water, ranging from a planar wall to viruses. In most cases some ion gets pulled away from the surface while some oppositely charged group, chemically bounded to the surface in question, stays behind. The ions leaving the surface are referred to as *counter-ions*. In this situation the counter-ions, as well as other charged particles residing in the system, will be attracted to the surface that carries an opposite charge. At the same time, however, the entropy wants to be maximal striving to a homogeneous

distribution of the ions. This clash of electrostatic versus entropic forces leads to some rather interesting physics. The equilibrium balances between entropy and electrostatics leads to the forming of an *electric double layer*. This double layer consists of a localized (say at $z = 0$) surface charge and a cloud of distributed ions.

4.1 Physical situation

Interactions between charged surfaces are important in many areas of (applied) physics. Many different theories have been developed in order to incorporate these interactions in many body systems. A convenient approximation is given by considering the ions as being dissolved in a structureless solvent with fixed dielectric constant ϵ. In this chapter the ions are considered point like with fixed valencies. This simplification is captured by the Poisson-Boltzmann equation, by means of a non-linear differential equation. A convenient representation of Poisson-Boltzmann theory turns out to be captured by classical DFT. We will consider point-like ions of charges $\pm e$ dissolved in a continuous medium with dielectric constant ϵ at fixed temperature T. The system is confined to a volume V. We consider the fluid of dissolved ions to be in contact with a at this point unspecified charge distribution $eq(\mathbf{r})$. Later on we will consider g the density profiles of the cations and anions, respectively $\rho_{\pm}(\mathbf{r})$. We will use the DFT framework as developed in chapter 3 and consider the system grand canonically. We incorporate hard core interactions in the Hamiltonian, reflecting the fact that ions are unable to penetrate the (fixed) background charge distribution.

A mixture of N_+ cations and N_- anions has a Hamiltonian of the form

$$H_{ionic} = K_{tot} + \Phi(\mathbf{r}_{+i}, \mathbf{r}_{-i}) + \mathcal{V}(\mathbf{r}_{+i}, \mathbf{r}_{-i}). \tag{4.1}$$

We will consider the interparticle interaction to be of the hard-sphere kind, leaving us with the following explicit expressions for the terms of Eq.(4.1)

$$K_{tot} = \sum_{i=1}^{N+} \frac{\mathbf{p}_{+i}}{2m_+} + \sum_{i=1}^{N-} \frac{\mathbf{p}_{-i}}{2m_-}. \tag{4.2}$$

For the sum of the kinetic energies of the respectively cations and anions. And

$$\Phi = \sum_{j=1}^{N+}\sum_{i=1}^{N-} \phi(|\mathbf{r}_{+j} - \mathbf{r}_{-i}|) + \sum_{i<j} \phi(|\mathbf{r}_{+j} - \mathbf{r}_{+i}|) + \sum_{i<j} \phi(|\mathbf{r}_{-j} - \mathbf{r}_{-i}|) \tag{4.3}$$

for the interparticle interaction, where ϕ denotes the hard-sphere repulsion if the particles overlap, and the Coulombic potential at larger distances:

$$\phi(r_{ij} = |\mathbf{r}_i - \mathbf{r}_j|) = \begin{cases} \infty & r_{ij} < r_{\pm} + r'_{\pm} \\ \frac{e^2}{4\pi\epsilon_0} \frac{Z_i Z_j}{|\mathbf{r}_i - \mathbf{r}_j|} & r_{ij} \geq r_{\pm} + r'_{\pm}. \end{cases} \tag{4.4}$$

Here $r_{\pm}$ denotes the particle radii of the cations and anions respectively. The coulombic part of the inter-particle interaction gives rise to a length scale in the system known as the *Bjerrum length*, λ_b, the length at which the electrostatic energy between two ions is

k_bT. It is defined as $\lambda_b = e^2/(4\pi\epsilon k_BT)$. The external potential takes on the following form

$$\mathcal{V} = \sum_i^{N+} V_+(\mathbf{r}_{+i}) + \sum_j^{N-} V_-(\mathbf{r}_{-j}), \tag{4.5}$$

where the external potential is the term containing the interactions between all the free ions in the solvent and the (at this point unspecified) fixed background charges. Here $V_\pm$ is given by

$$V_\pm = V_b + Z_\pm k_BT\lambda_B \int d\mathbf{r}' \frac{\pm q(\mathbf{r}')}{|\mathbf{r}-\mathbf{r}'|}, \tag{4.6}$$

where $q(\mathbf{r})$ is the fixed charge distribution and the V_b is a hard-sphere like potential incorporating the fact that the ions cannot penetrate the fixed charge distribution (e.g. the ions cannot just penetrate a charged wall, or charged colloids suspended in the solvent).

4.2 Coulomb Interactions

We can apply a mean field approximation to give an expression for excess free energy functional. Using the exact ideal gas functional as a reference point for both the cations and the anions Eq.(2.39) we can write [5]

$$\begin{aligned}\mathcal{F}[\rho_+,\rho_-] = kT\sum_\pm \int d\mathbf{r}\rho_\pm(\mathbf{r})\left(-1+\ln\rho_\pm(\mathbf{r})\Lambda_\pm^3\right) \\ + \frac{k_BT\lambda_B}{2}\int\int d\mathbf{r}d\mathbf{r}' \frac{(\rho_+(\mathbf{r})-\rho_-(\mathbf{r})+q(\mathbf{r}))\,(\rho_+(\mathbf{r}')-\rho_-(\mathbf{r}')+q(\mathbf{r}'))}{|\mathbf{r}-\mathbf{r}'|}.\end{aligned} \tag{4.7}$$

With the second term representing the mean field ionic interactions. At this point we introduce the dimensionless function

$$\phi(\mathbf{r}) = \int d\mathbf{r}'\lambda_B \frac{q(\mathbf{r}')+\rho_+(\mathbf{r}')-\rho_-(\mathbf{r}')}{|\mathbf{r}-\mathbf{r}'|}, \tag{4.8}$$

which can be seen as the local dimensionless electrostatic potential. Using this definition we can write the mean field coulomb functional as

$$\mathcal{F}_{MFC}[\rho_+,\rho_-] = \frac{k_BT\lambda_B}{2}\int d\mathbf{r}Q(\mathbf{r})\phi(\mathbf{r}), \tag{4.9}$$

where $Q(\mathbf{r}) = \rho_+(\mathbf{r}) - \rho_-(\mathbf{r}) + q(\mathbf{r})$ is the total charge density, consdering both ionic and background contributions. We note that with this choice we view the charged boundary as intrinsic to the system. In the case of planar electrodes this charge density arises from a certain applied potential Φ. With this choice only the hard-core like interactions V_b appear explicitly as the external potential. The coulombic interactions between the ions and the fixed charge distribution are incorporated in the coulombic mean field functional. The grand potential functional takes on the general form $\Omega = \Omega_{id} + \Omega_\Phi + \Omega_\mathcal{V}$.

Using the fact that $\mu_\pm = kT\ln\rho_b\Lambda_\pm^3$ with ρ_b the bulk density of both ionic species we can write

$$
\begin{aligned}
\Omega_{\mathcal{V}} &= \sum_{\pm} \int\int d\mathbf{r} d\mathbf{r}' \lambda_b \frac{q(\mathbf{r})\rho_{\pm}(\mathbf{r}')}{|\mathbf{r}-\mathbf{r}'|} + \int d\mathbf{r}\,(\rho_+(\mathbf{r}) + \rho_-(\mathbf{r}))\, V_b(\nabla), \\
\Omega_{\Phi} &= \sum_{\pm}\sum_{\pm} \frac{1}{2} \int\int d\mathbf{r} d\mathbf{r}' \lambda_B \frac{\rho_{\pm}(\mathbf{r})\rho_{\pm'}(\mathbf{r}')}{|\mathbf{r}-\mathbf{r}'|}, \\
\Omega_{id} &= k_b T \sum_{\pm} \int d\mathbf{r} \rho_{\pm}(\mathbf{r}) \left(\ln \frac{\rho_{\pm}(\mathbf{r})}{\rho_b} - 1 \right).
\end{aligned}
\tag{4.10}
$$

Plugging in these expressions the explicit form for the grand potential functional reads

$$
\begin{aligned}
\Omega[\rho_{\pm}] = \Omega_{id} &+ \frac{1}{2} kT \int d\mathbf{r}\,(q(\mathbf{r}) + \rho_+(\mathbf{r}) - \rho_-(\mathbf{r}))\,\phi(\mathbf{r}) \\
&+ \int d\mathbf{r}\,(\rho_+(\mathbf{r}) + \rho_-(\mathbf{r}))\, V_b(\mathbf{r}).
\end{aligned}
\tag{4.11}
$$

Functional differentiation of this grand potential yields the following expression

$$
\begin{aligned}
\beta \frac{\delta\Omega[\rho_{\pm}]}{\delta\rho_{\pm}(\mathbf{r})} &= \frac{\delta\Omega_{id}}{\delta\rho_{\pm}} \pm \frac{1}{2} kT 2\phi(\mathbf{r}) + \rho_{\pm} V_b(\mathbf{r}) \\
&= \ln \frac{\rho_{\pm}}{\rho_s} \pm \phi(\mathbf{r}) + \rho_{\pm} V_b(\mathbf{r})\beta.
\end{aligned}
\tag{4.12}
$$

In the absence of any other interactions we can write the equilibrium condition as a Boltzmann distribution

$$
\rho_{\pm}(\mathbf{r}) = \begin{cases} \rho_s \exp[\pm\phi(\mathbf{r})] & \beta V_b(\mathbf{r}) = 0 \\ 0 & \beta V_b(\mathbf{r}) = \infty \end{cases}
\tag{4.13}
$$

Using the identity $\nabla^2 r^{-1} = -4\pi\delta(\mathbf{r})$ it is possible to invert the Coulomb equation Eq. (4.8) and obtain its differential form

$$
\nabla^2 \phi(\mathbf{r}) = -4\pi\lambda_B Q(\mathbf{r}).
\tag{4.14}
$$

Equation (4.13) is useful because it can be used as a starting point in the Picard iteration.

4.3 Beyond Mean Field

As discussed above, the easiest way to incorporate electrostatic interactions in a DFT framework is by using the mean field coulomb functional Eq.(4.9) where the dimensionless electrostatic potential is solved by means of Eq. (4.14). This functional, however, provides accurate results only for relatively low bulk densities. For larger bulk densities we have to take ionic correlations into consideration [1].

[1] This work is based on work in progress by Peter Cats. For a more in depth look one can also look at [17]

Mean Spherical Approximation

The mean spherical approximation is a closure needed to solve the Ornstein-Zernike equation Eq. (2.56). Specifically this closure reads $g_{ij} = 0$ for $r < R_i + R_j$ and $\beta c_{ij} = -z_i z_j \lambda_b / r$ for $r > R_i + R_j$. Using this closure one obtains the direct and total correlation function Eq. (2.56).

4.3.1 MSAc

The first functional going beyond ordinary mean field takes the excess direct correlation function $\Delta c(r_i; \rho_b)$ found when solving the OZ-equation with the MSA closure and implements it in a mean field manner

$$\mathcal{F}_{MSAc} = -\frac{1}{2}\beta \sum_{ij} \int d\mathbf{r} \int d\mathbf{r}' \rho_i(d\mathbf{r}) \Delta c_{ij}(|\mathbf{r} - \mathbf{r}'|; \rho_b) \rho_j(\mathbf{r}'), \tag{4.15}$$

taking into account short range ionic correlations through the MSA direct correlation function $c_{ij}(r_i; \rho_b)$.

4.3.2 MSAu

Going one step beyond this extended mean field approach means using the direct correlation function to find the total internal energy of the bulk via the energy route to thermodynamics. We can consider the charged particles as being spheres with a homogeneous charge distribution, instead of charged points. This is implemented by using a set of weighted densities, of similar form as the ones we have seen before in the development of Rosenfelds FMT. This gives rise to a functional using mean field, and the direct correlation and internal energy from the system. This functional will be referred to as MSAu.

Chapter 5

Differential capacitance of room temperature ionic liquids using DFT; the influence of dispersion forces

Describing ionic density profiles under typical room temperature ionic liquid (RTIL) conditions in cavities ranging from 2 nm to 60 nm has been a great challenge for some time now. In this chapter we will examine the influence of dispersion forces on the electrochemical properties of ionic liquids in contact with planar electrodes. We will do this by numerically solving the Euler-Lagrange equations predicted by DFT using Matlab. The basic idea behind the code will be explained in the first section, after which we will look at some of the results obtained from it. We will consider density profiles, surface charge densities and differential capacitance of a symmetric RTIL. Density functional theory predicts strong layering of ions at high surface potentials. We will find that the transition of a camel- to a bell-shaped differential capacitance curve is highly dependent on the dispersion forces between the ions and the electrode surface. Dispersive attraction between particles and the electrode surface leads to ionic accumulation in the vicinity of the electrode for low surface potentials. We will also consider the role of inter-particle dispersion in this process.

5.1 Introduction

Room temperature ionic liquids (RTIL's) are salts with melting points at or below 100 °C. They have been attracting increased attention from the scientific community, not in the least place because of their potential for electrochemical energy storage. Their potential as electrolytes in batteries and capacitors is currently being investigated, both theoretically and experimentally. Due to the low dielectric constant of molten salts the electrostatic correlations between ions is much higher than in the usual aqueous electrolytes, making this regime a great theoretical challenge. For the development of energy devices, however, a profound understanding of the electric double layer (EDL) properties, like surface charge density and differential capacitance, of ionic liquids is needed. All properties of the EDL one would be interested in can be calculated from the structure of the IL in its geometric confinement, that is, the amount of layering of the ions as predicted by their density

profiles.

For some time the influence of HS-interactions on the interfacial properties of RTIL's has been known. A fast decay in differential capacitance for increasing absolute values of surface potential can be attributed to maximal packing of counter-ions at the electrode surface. Direct measurements of the differential capacitance 1-butyl-3-methyl-imidazolium hexafluorphospate and N-butyl-N-methyl-pyrrolidium hexafluorphosphate and more recent work using chronoamperometry on both dilute and pure 1-ethyl-3-methylimidazolium bis(trifluoromethylsulfonyl)imide confirm this decay [22, 23]. Both studies show a minimum in the differential capacitance around a surface charge of 0 V, surrounded by two maxima at non-zero values of electrode potential, giving rise to a camel-shaped capacitance curve. In addition, this curve is found to be asymmetric in the case that cationic and anionic radii differ.

Lamperski *et al.* showed that computer simulations and modified Poisson-Boltzmann theory predict a camel-shaped capacitance curve for a dilute, binary mixture of charged hard spheres [24]. They also predict a transition from a camel-to-bell shaped differential capacitance curve as the ionic packing fraction increases. This has been observed in the experiment of [23]. Fedorov and Koryshev used Monte-Carlo (MC) simulations as well as molecular dynamics to simulate a charged hard sphere model and also found a camel-to-bell transition of the differential capacitance curve [25]. Jiang *et al.* predicted a transition from camel-to-bell shaped differential capacitance curves using DFT, but they did not include the attractive part of Lennard-Jones [26].

Despite these numerous efforts in trying to understand the interfacial properties of ionic liquids at charged surfaces, a complete theory for the observed transitions has not yet been developed. Lauw *et al.* used a mean field theory to study the interfacial properties of the RTIL double layer, and found that a varying dielectric constant may attribute to a change in differential capacitance [27]. Monte-Carlo simulations performed by Vatamanu *et al.* to investigate temperature dependence of the differential capacitance also found camel-shaped curves [28]. Lot *et al.* showed using MC simulations that the bell-shape can be attributed to a strong interaction between a metal electrode and counter-ions, but experimental work has also found camel-shaped differential capacitance curves for these specific electrodes [29]. Trulsson *et al.* attributed the camel-shape due to loss of dispersion near the electrodes using MC simulations [30].

The standard theory for describing the behaviour of aqueous solutions containing mobile ions is Gouy-Chapman (GC) theory. In GC-theory it is assumed ions are point like particles that only interact through electrostatic coulomb interactions. Within this framework counter- and co-ionic density profiles are predicted to decay and respectively increase monotonically from its contact peak until it reaches its bulk value. Furthermore, this model predicts a differential capacitance curve with a U-shape, reaching its minimum value at a wall potential of $\phi_0 = 0$ V. When we look at ionic liquids, the strong ionic correlations will lead to a very different structure of the EDL. A commonly used theory in predicting the EDL-properties within this regime is modified Poisson-Boltzmann theory, incorporating excluded volume effect and in some cases even ionic correlations. This theory predicts bell- or camel-shaped differential capacitance curves, reaching maximum values at the point of zero surface charge.

Just recently the scientific community started applying density functional theory in the realm of ionic liquids. We will use this framework to study the behaviour of ionic

liquids in a slit pore of a porous electrode and in particular, we will investigate the role of dispersion forces, of both inter-particle kind as well as between the particles and the electrode surface, on the electrochemical properties of the RTIL EDL.

5.2 Model and method

The ionic concentration of the system is defined in terms of the ionic packing fraction $\eta = 4\pi(\rho_-^b R_-^3 + \rho_+^b R_+^3)/3$, where $\rho_\pm^b$ are the ionic bulk densities and $R_\pm$ the ionic radii. We will consider two planar electrodes separated by a distance $L = 6$ nm at potentials $\phi_0^\pm$. We then use the term counter-ions for the ions carrying opposite sign charge to the electrode and co-ions carrying the same sign. We use the theoretical model of classical density functional theory in order to describe this system. For the readers convenience we will recall the most important results from chapter 2, 3 and 4, devoted to the general development of DFT, as well as the sections devoted to the approximation of certain free energy functionals, respectively. Classical density functional theory is formulated in grand canonical setting, where the temperature T, volume V and chemical potential $\mu_\pm$ of all the interacting species are specified. The grand potential is a functional of the ionic density profiles

$$\Omega[\rho_+(\mathbf{r}), \rho_-(\mathbf{r})] = \mathcal{F}[\rho_+(\mathbf{r}), \rho_-(\mathbf{r})] - \sum_\pm \int d\mathbf{r}(\mu_\pm - V_\pm(\mathbf{r}))\rho_\pm(\mathbf{r}). \tag{5.1}$$

This functional, Eq. (5.1), is minimized by the equilibrium ionic density profiles $\rho_\pm^0$, and at the equilibrium density yields the grand potential of the system. The Helmholtz free energy functional $\mathcal{F}$, for our purpose, consists of several terms

$$\mathcal{F}[\rho(\mathbf{r})] = \mathcal{F}_{id}[\rho(\mathbf{r})] + \mathcal{F}_{HS}[\rho(\mathbf{r})] + \mathcal{F}_{ele}[\rho(\mathbf{r})] + \mathcal{F}_{att}[\rho(\mathbf{r})], \tag{5.2}$$

where the terms on the right hand side represent the ideal gas contribution, the hard-sphere repulsion, electrostatic interaction and the mean field attractive term of the Lennard-Jones potential, respectively. We mention once again that the *electrostatic interactions* between the wall potential and the ions are incorporated in the coulombic functional. Thus, in Eq.(5.1) V_i represents only the steric repulsion between the electrodes and the ions or, as we will see later, the Steele potential incorporating dispersion between the particles and the electrode surface.

The ideal gas term is known exactly and is given by Eq. (2.38). We use here the tensorial version of the WBII for the hard-sphere functional, see (2.38). For the coulombic interactions we have two different functionals going beyond mean field. The MSAc functional is a mean field like functional of the analytically known solution for the direct correlation function of a mixture of charged hard spheres. The MSAu functional takes this one step further, viewing particles as having a shell with a homogeneous charge distribution. The MSAu functional will be the most accurate functional for predicting structural and thermodynamic properties at high bulk densities.

Minimization of Eq. (5.1) with respect to the ionic density profiles produces a set of non-linear integral Euler-Lagrange equations that need to be solved numerically. In our geometry we are neglecting size effects leading to translation invariance in two directions, leaving us with density profiles only depending on the coordinate perpendicular to the

planar surface. At the same time the Poisson equation (4.14) is solved for the dimensionless electrostatic potential $\phi(z)$. The surface charge density σ of the electronic walls can by calculated by means of Gauss's law of divergence, $\nabla \cdot E = \rho/4\pi\epsilon_0$. Comparing this expression with the Poisson-equation and evaluating at $z = 0$ yields the one dimensional form $\phi'(0) = -4\pi\lambda_B\sigma$ where λ_B denotes the Bjerrum length. Functional minimization of (5.1) yields the physical density profile $\rho(z)$. The thermodynamics follows from Ω evaluated at $\rho(z)$, yielding the grand potential.

The equations are solved using a Picard-Iteration method in *Matlab*. For a brief explanation of the Picard iteration method see Appendix D. The differential capacitance per unit area is calculated by a numerical derivative of the surface charge density σ viewed as function of the surface potential ϕ_0

$$C_d = \frac{\partial\sigma}{\partial\phi_0}. \tag{5.3}$$

The Lennard-Jones attraction between the particles and the electrode surface is incorporated via the Steele 10-4-3 potential

$$V_s(z) = \epsilon_w \left[\frac{2}{5}\left(\frac{\sigma_w}{z}\right)^{10} - \left(\frac{\sigma_w}{z}\right)^{4} - \frac{\sigma_2^4}{3\Delta(z+0.61\Delta)^3} \right]. \tag{5.4}$$

For a carbon electrode the Steele-parameters are related to the Lennard-Jones parameters via [20]

$$\sigma_w = 0.903\sigma, \epsilon_w = 12\epsilon_p, \Delta = 0.8044\sigma. \tag{5.5}$$

Here ϵ_p is the inter-particle strength parameter in the LJ-potential and σ is the distance for which the inter-particle potential is zero. For the shape of this potential see fig 5.1 and for a schematic drawing of the Steele potential see fig 5.2.

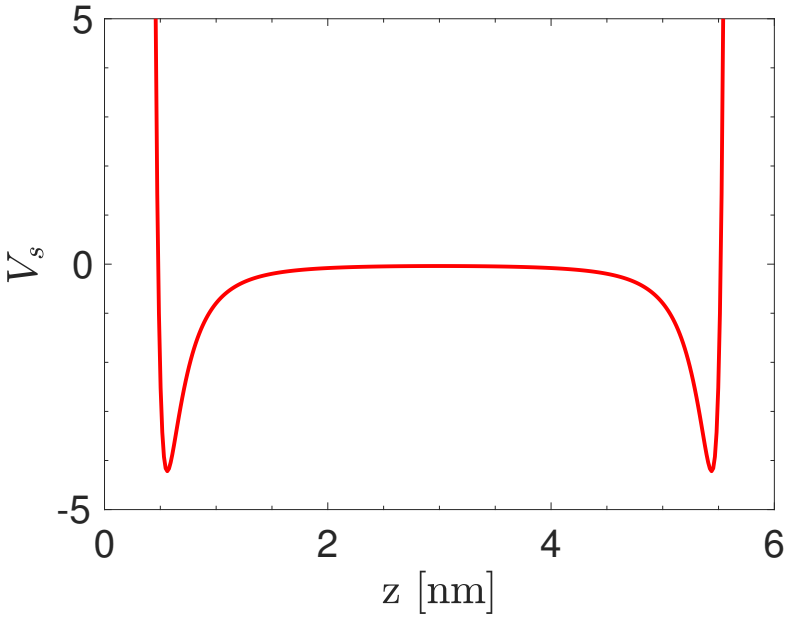

Figure 5.1: The Steele potential of Eq. 5.4 plotted as function of z for values of 5.5.

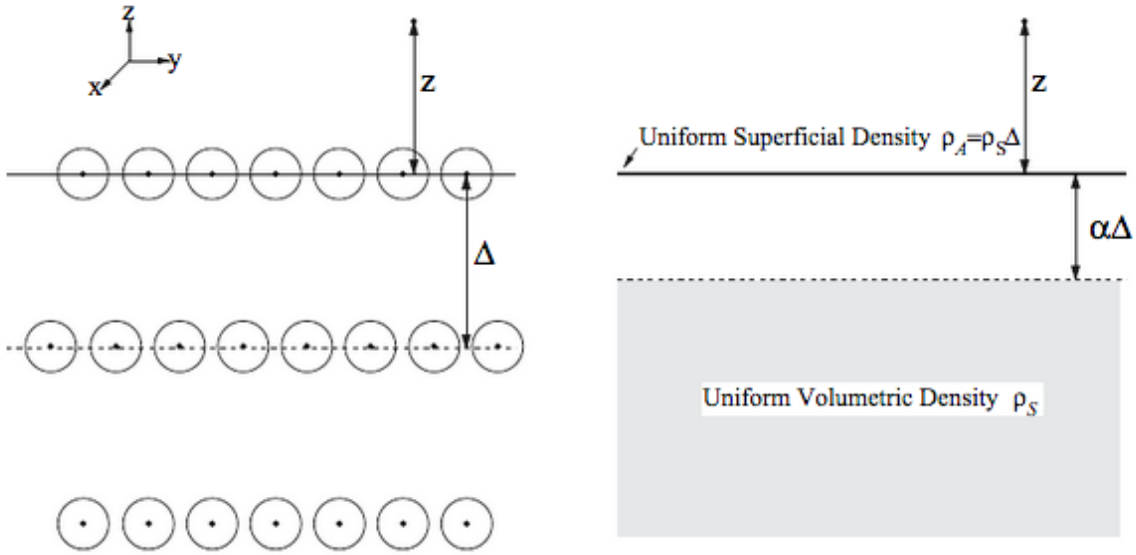

Figure 5.2: Schematic drawing for the explanation of the Steele 10-4-3 potential as considered for a carbon electrode. The left shows three crystalline planes of graphitic carbon, each separated by Δ*. The first plane is exposed to fluid molecules located at z relative to the first plane. The right shows the material that is effectively modeled by the Steele 10-4-3 potential. The first component is a continuum planar layer with areal density* $\rho_s\Delta$*. The second component is a continuum slab with volume density* ρ_s *that begins at* 0.61Δ *from the exposed layer and continues infinitely in the z-direction. Picture and caption taken from Scientific Figure on ResearchGate -* ***"Extension of the Steele 10-4-3 potential for adsorption calculations in cylindrical, spherical, and other pore geometries.***

Excluding attractive LJ-interactions between the ions and the electrode while keeping inter-particle dispersion forces can be accomplished by setting ϵ_w to 0. We will consider different values for ϵ_w, ranging from absence of dispersion to the value for graphitic carbon. The repulsive part of the Lennard-Jones interaction, that is based on FMT, uses an effective hard-sphere diameter that generally is not the same as the bare atomic radii. The effective particle diameter σ is calculated in the same manner as in the work of Tang and Wu [21].

5.3 Results

We consider a symmetric model in which the cationic and anionic particle radii are $R = R_+ = R_- = 0.3$ nm. The dielectric constant is fixed at $\epsilon = 10$, common for ionic liquids [19]. The calculations are performed at a temperature of 373.15 K, yielding a Bjerrum length of 4.1 nm. We consider a slit pore of total length $L = 6$ nm. When incorporating inter-particle dispersion the Lennard-Jones parameter is set at $\epsilon_p = 0.5$ k_bT, similar to the the value Trulsson *et al.* used in their MC simulations [30].

Figure 5.3 shows the surface charge density as a function of the surface potential for packing fractions ranging from $\eta = 0.05$ to $\eta = 0.4$ (0.2 M to 3 M). The results are plotted for different values of dispersion between the particles and the electrode surface, respectively $\epsilon_w = 6$ (comparable to graphitic carbon), $\epsilon_w = 1$, $\epsilon_w = 0.1$ and $\epsilon_w = 0$. In all

plots the inter-particle dispersion is $\epsilon_p = 0.5$. Because the cations and anions have the same size these plots are symmetric in the origin. In all cases the surface charge density increases monotonically with increasing surface potential. At high absolute values of the surface potential the surface charge seems to increase linearly regardless of the strength of LJ-interaction and packing fraction. The slope of this linear part depends slightly on the strength of the dispersion. For $\epsilon_w = 0$, $\epsilon_w = 0.1$ we observe the slopes being roughly the same in the linear part. For $\epsilon_w = 1$ and $\epsilon_w = 6$ the slopes are slightly less, with the latter having the lowest value. Striking is the increasing similarity for the curves with $\epsilon_w = 6$ and $\epsilon_w = 1$ at packing fractions of $\eta = 0.2$, $\eta = 0.3$ and $\eta = 0.4$ around the point of $\phi_0 = 0$ (fig. 5.3 (c) - (d)). In the cases that $\epsilon_w = 0$ and $\epsilon_w = 0.1$ we see a clear transition in shape of the curve for low surface potentials when the packing fraction increases. As can be seen in fig. 5.3 (c) - (e) the slopes of these curves increase around the point of zero potential as the packing fraction increases. In fig. 5.3 (a) and fig. 5.3 (b) a noticeable change in curvature can be observed as compared to fig. 5.3 (c) - (e). The slope increases first, as phi_0 approaches zero, then decreases a bit, to increase again till it flattens out to the linear tail.

In figure 5.4 the differential capacitance per unit area is plotted for the same circumstances as in figure 5.3. There is a clear cut distinction in the shape of the differential capacitance between the lowest values and the highest values of the energy parameter. For $\epsilon_w = 0$ and $\epsilon_w = 0.1$ a transition from a camel-shaped to a bell-shaped curve can be observed at a packing fraction of $\eta = 0.3$ (fig. 5.4 (d)). For $\epsilon = 6$ we see this transition taking place at a significantly lower packing fraction of $\eta = 0.05$. The trend seems to be that the lower the energy parameter ϵ_w, the later C_d seems to transit between a camel-shape to a bell-shape curve when increasing the packing fraction. Quantitatively, the value of the maximum of C_d for $\epsilon_w = 0$ and $\epsilon_w = 0.1$ are significantly different, with the former establishing higher peaks. In contrast with the regime of greater dispersive attraction, $\epsilon_w = 1$ and $\epsilon_w = 6$, where the latter establishes higher peaks at packing fractions ranging from $\eta = 0.05$ to $\eta = 0.3$. In accordance with the steepness of the surface charge density in the linear regime, as discussed above, we observe that for $\epsilon_w = 0$ and $\epsilon_w = 0.1$ the curves reach the same value for C_d at high absolute values of the surface potential. For $\epsilon_w = 1$ and $\epsilon_w = 6$ there is a small discrepancy, with the latter one establishing the lowest value. As observed above, for low surface potentials $\epsilon_w = 1$ and $\epsilon_w = 6$ curves start to look more similar.

Figure 5.5 shows the surface charge density for the same parameter regime, with the only difference being that the inter-particle dispersion is set to $\epsilon_p = 0$. It can be seen that in this case the difference between $\epsilon_w = 6$ and $\epsilon_w = 1$ is even less significant as compared to the case in which $\epsilon_p = 0.5$ around the point of zero surface potential. At high absolute values for the surface potential the surface charge density seems to increase linearly as well for all packing fractions. For low values of ϵ_w the curves reach the same slope, slightly higher than the slope for the higher values of ϵ_w and roughly the same absolute value of steepness as for the case of $\epsilon_p = 0.5$.

Figure 5.6 shows the differential capacitance per unit area for this situation. For $\epsilon_w = 0$ and $\epsilon_w = 0.1$ the transition from a camel-shape to a bell-shape takes place at a packing fraction of $\eta = 0.2$, slightly lower than the case with $\epsilon_p = 0.5$. We see that even at the lowest packing fraction of $\eta = 0.05$ the curve for $\epsilon_w = 6$ has not yet transitioned to a camel-shape, whereas this transition is already observed when $\epsilon_p = 0.5$. At packing

fractions of $\eta = 0.4$ and $\eta = 0.3$ the peaks for $\epsilon_w = 0$ and $\epsilon_w = 0.1$ are significantly higher as compared to the case in which $\epsilon_p = 0$. For lower packing fraction this effect diminishes, and it can even be observed the peaks are becoming lower as compared to the case in which $\epsilon_p = 0.5$.

Figure 5.7 shows the co-ionic (red) and counter-ionic (black) density profiles normalized to bulk for different values of the wall energy parameter ϵ_w and inter-particle energy parameter ϵ_p at a packing fraction of $\eta = 0.05$. These plots represent the situation at a wall potential of $\phi_0 = 0.1$ V. Since we are considering a symmetric system, these plots would have looked the same for the negative potential regime, only with the role of co- and counter-ions reversed. At this low value of the surface potential and low packing fraction the dispersion forces play a relatively big role as compared to the electrostatic interactions. We observe in fig. 5.7 (a) that counter-ionic contact peaks, and the co-ionic peak thereafter, decrease when ϵ_p diminishes. This is at a relatively high value of ϵ_w. In fig. 5.7 (b) - (d) this trend reverses, with the respective peaks increasing as ϵ_p diminishes. This difference is most striking when $\epsilon_w = 0$ (5.7 (d)). At $\epsilon_w = 6$ we find a more profound layering of ions, extending farther in the bulk than for the lower values of ϵ_w, where the counter-ionic peaks seem to decay exponentially, quickly reaching the bulk value. In figure 5.8 the density profiles have been plotted for the same parameters, except this time for a packing fraction of $\eta = 0.4$. As compared to the figures for $\eta = 0.05$ it is immediate that the ionic layering is stronger in this case. In all cases the contact-peaks rise when ϵ_p diminishes.

5.4 Discussion

As Kornyshev *et al.* have shown, the decay of the differential capacitance for high absolute values of the surface potential can be explained by means of saturation effects, that is, maximal packing of counter-ions at the electrode surface [31]. When dispersion forces between the particles and the electrode surface play a less significant role, that is, $\epsilon_w = 0$ or $\epsilon_w = 0.1$, the surface charge density is more dependent on the electrostatic forces in play. This has the effect that when the surface potential increases the surface charge density is bound to increase more rapidly than in the case of strong dispersion forces between the particles and the electrode surface. This will in general yield higher values of the differential capacitance throughout the electrochemical window in which we consider the IL, as we have observed in our results.

We would like to predict the general appearance of the differential capacitance, and predict how the values and the shape of the curves change as we change the system parameters. When the electrode surface is almost neutral, ions will be depleted in the vicinity of the electrode as opposed to high surface potentials. With this depletion the surface charge density will change relatively slowly with changing potentials, yielding a minimum for the differential capacitance. The more depleted the ions will be, the lower C_d will be. When the wall potential increases, counter-ions will accumulate in the vicinity of the electrode surface. With relatively many ions being able to respond to changes in the potential, the surface charge density will change relatively quickly with changing potentials. When the IL is considered this way, we would expect U-shape differential capacitance curves, reaching a minimum at a surface potential of 0 V. However, when

the surface potential increases more ions will accumulate in the vicinity of the electrode, leading to saturation effects. This limits the response of σ to a change of surface potential ϕ_0. At low densities this will lead to the camel-shaped curve, with a minimum of C_d at zero surface charge flanked by two maxima at non-zero values of surface potential. High packing fractions will naturally lead to a more saturated layer in the electrode vicinity, yielding the same limitation of change in σ for changing ϕ_0. This gives rise to the bell-shaped C_d curve, with a maximum at zero surface charge.

The value of the differential capacitance at at low absolute values of the surface potential depends highly on the amount of depletion and accumulation of ions in the vicinity of the electrode surface. The transitioning of the differential capacitance from bell-to-camel shape for $\epsilon_w = 0$ at a lower packing fraction as opposed to the case in which $\epsilon_w = 0.5$ can be understood now by means of the heuristics above. When the particles interact through the LJ-attraction the ions in the vicinity of the electrode will feel attraction from the bulk fluid, creating a depletion as opposed to when this inter-particle interaction is not taken into consideration. This is also confirmed by the density profiles at a packing fraction for $\eta = 0.1 - \eta = 0.4$, see figure 5.8 (here only $\eta = 0.4$ has been shown) and observe how the dashed contact-peaks have higher values than their solid counterparts.

For a packing fraction of $\eta = 0.05$ at a value for $\epsilon_w = 6$ we see that ions tend to accumulate when $\epsilon_p = 0.5$ as opposed to when ϵ_p diminishes. The strong attraction between the particles and the wall may create a layering of ions so strong that it attracts ions from the bulk, that is characterized by a relatively low density. This is confirmed by the curves for C_d, where for $\eta = 0.05$ the curves corresponding to $\epsilon_p = 0.5$ are higher than the same curves in the regime where $\epsilon_p = 0$.

When $\epsilon_p = 0.5$ the minimum of the differential capacitance for diminishing values of ϵ_w is significantly lower as opposed for the same curves when $\epsilon_p = 0$. This due to the greater amount of depletion of ions in the electrode vicinity as discusses above.

We can more explicitly look at the effect of ionic layering on C_d. This is particularly nice in the case where $\eta = 0.05$, for different values of ϵ_w as we see a difference between relatively strong layering fig. 5.7 (a) and exponentially decaying profiles fig. 5.7(c) - (d). In the absence of specific adsorption, the total differential capacitance C_t is related to the differential capacitance of the contact layer, the first layer of ions screening of the electrode potential, and the diffuse layer thereafter, by

$$\frac{1}{C_t} = \frac{1}{C_c} + \frac{1}{C_d}, \tag{5.6}$$

where C_c is the differential capacitance of the contact layer, and C_d of the diffuse layer. When the amount of layering increases, due to increasing surface potential and/or changing energy parameters ϵ_w and ϵ_p, C_d increases while C_c is relatively stable. At sufficiently high amounts of layering, C_d will become much greater than C_c. In that case C_t will be dominated by C_c. At a packing fraction of $\eta = 0.05$, for an interaction strength of $\epsilon_w = 6$, we observe a profound layering as compared to $\epsilon_w = 1$, $\epsilon_w = 0.1$ and $\epsilon_w = 0$. Looking at value of the differential capacitance per unit area for $\eta = 0.05$ at a value of $\phi_0 = 0.1$ V we observe that indeed the red curve, corresponding with $\epsilon_w = 6$ has the highest value of C_t, as C_t is more dominated by C_c.

In general, the bell-shape of the differential capacitance for strong dispersive inter-

actions between the particles and the wall remains qualitatively stable under decreasing packing fractions, that is, it only transitions to a camel-shape at packing fractions far below the same point of transition for much weaker dispersive attraction between the particles and the wall. This is because a LJ-like attraction with the wall increases the ionic accumulation (at low packing fractions and low surface potentials). This kind of interaction makes the C_d-curve qualitatively stable.

5.5 Conclusion and Outlook

Our results, obtained by applying the framework of DFT in the situation for which ionic liquids are confined in a slit pore, modeled as two planar electrodes, indicate that the electrochemical properties of the EDL that forms are strongly dependent on dispersion forces, both of inter-particle kind as well as between particles and the wall. Since the minimum of differential capacitance is due to depletion of the IL near the electrode surface when the potential reaches zero, the effect of attractive LJ attractions plays a crucial role in determining the electrochemical properties of the EDL. Since a LJ-like attraction with the wall increases the ionic accumulation (at low packing fractions and low surface potentials) this kind of interaction makes the C_d curve qualitatively stable, transitioning from a bell-shape to a camel-shape at lower values of packing fractions η as opposed to when there is no LJ-attraction with the wall. The fact that the amount of dispersive attraction between the particles and the electrode surface plays such a prominent role in the determining of the electrochemical properties of the IL EDL, in principle, means that these properties can be fine-tuned to perfection by using appropriate electrode surfaces.

It is, however, hard to draw conclusions of the sole importance of dispersive attraction on the EDL properties of real ionic liquids. The model we consider is still crude, and does not take into consideration the structure of the ionic liquids. Zhang *et al.* established the fact that specific adsorption is of paramount importance for the shape of C_d [22]. This is due to certain chemical groups, like aromatic rings, being able to squeeze and allow for the ions to more closely approach the electrode surface. Varying ionic sizes is bound to have a profound effect on the electrochemical properties as well. Smaller ions can more efficiently screen of the electrode charges. We have only considered a symmetric mixture in which cations and anions are modelled as having the same radii. Interesting would be to use DFT to make predictions for an asymmetric mixture as well. More examples of experimental measurements of the electrochemical properties of ionic liquids are sparse. In the experiments that have been done, both camel-humped shapes as well as bell-shaped curves for the differential capacitance have been observed [22, 23, 32, 33].

Although this crude model fails to capture the finer microscopic structure of the ionic liquid, the predictions made are still relevant to RTIL's. Ionic radii of 0.3 nm are well in the regime of commonly encountered room temperature ionic liquids. The dielectric constant of $\epsilon = 10$ is of the same order as many common molten salts. Fact that DFT predicts a transition from bell-shape to camel-shape that is highly dependent on the amount of dispersive attraction, a transition that has been observed in experiments, indicates that also in the regime of molten salts DFT proves to be a powerful tool in predicting structural and thermodynamic properties of nano-scale systems.

For further research it would be interesting to use DFT to dissect the importance of

various system parameters on the electrochemical properties of RTIL's EDL's. Extensions to different regimes are also possible. While DFT has been widely used in the making of theoretical predictions of aqueous salt solutions in contact with electrode surfaces, solutions characterized by a high dielectric constant and relatively low temperature, it would be interesting to revisit these physical situations and look at the role of dispersion. Also molten salts, ionic liquids characterized by their relatively high melting point, will provide an interesting physical regime in which this powerful tool can be applied.

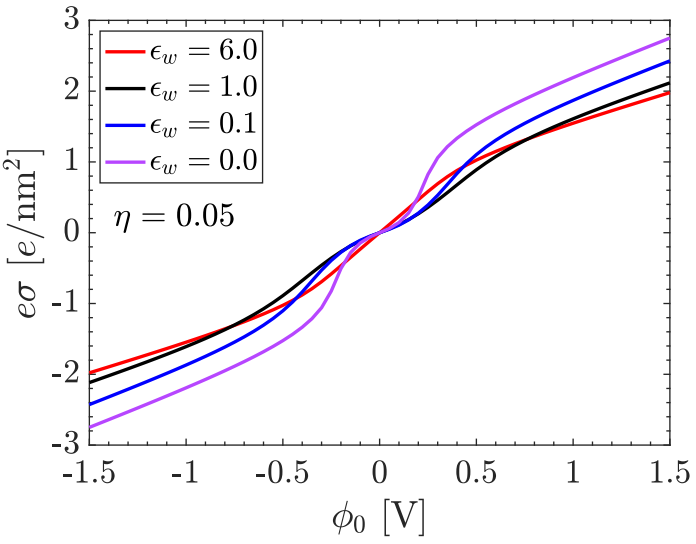

(a)

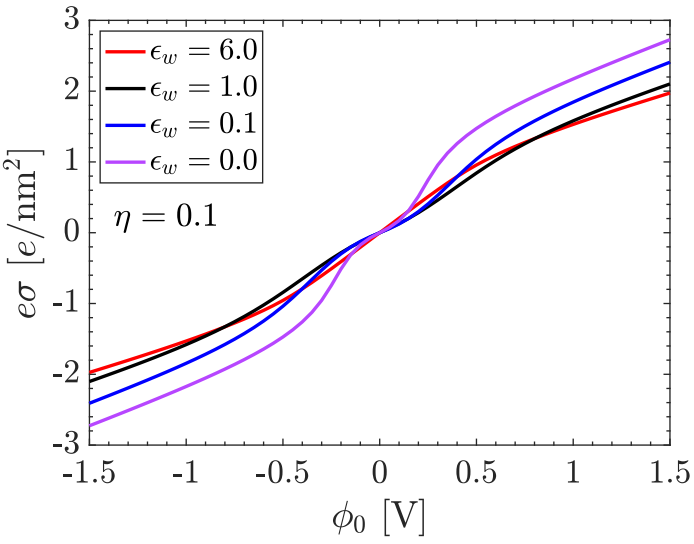

(b)

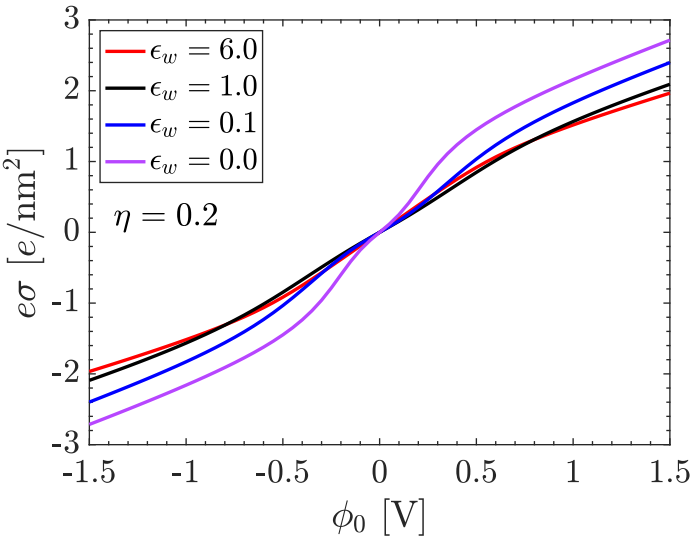

(c)

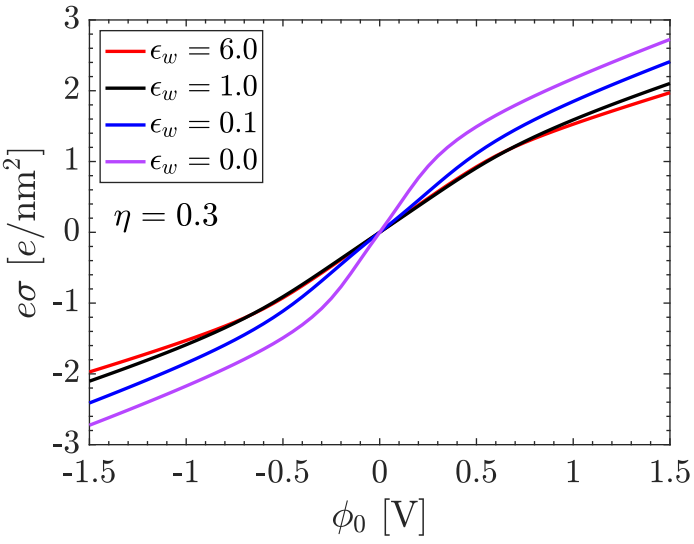

(d)

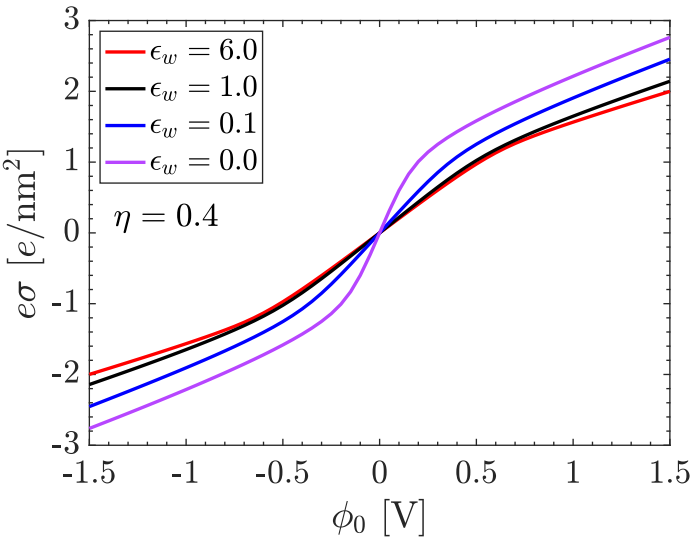

(e)

Figure 5.3: Surface charge densities as a function of the electrode potential for packing fractions of $\eta = 0.05$ (a), $\eta = 0.1$ (b), $\eta = 0.2$ (c), $\eta = 0.3$ (d) and $\eta = 0.4$ (e). The plots are made for values of ϵ_w (in units of k_bT) of $\epsilon_w = 6$ (red), $\epsilon_w = 1$ (black), $\epsilon_w = 0.1$ (blue) and $\epsilon_w = 0$ (violet). All graphs are made for an inter-particle attraction strength of $\epsilon_p = 0.5k_bT$.

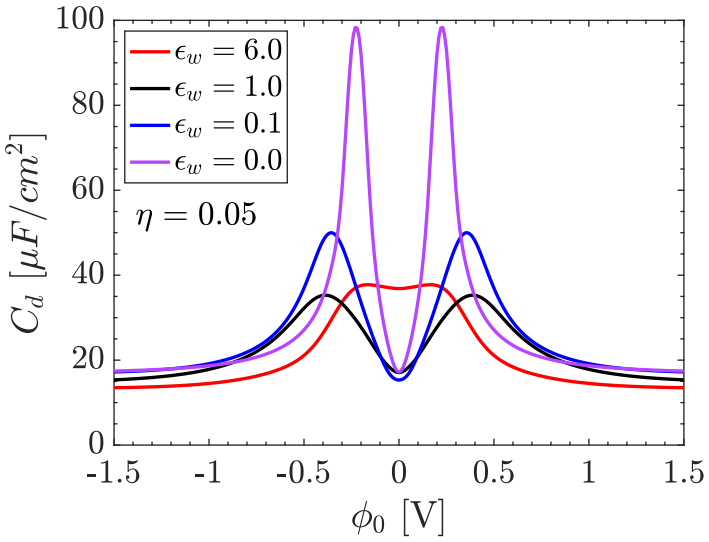

(a)

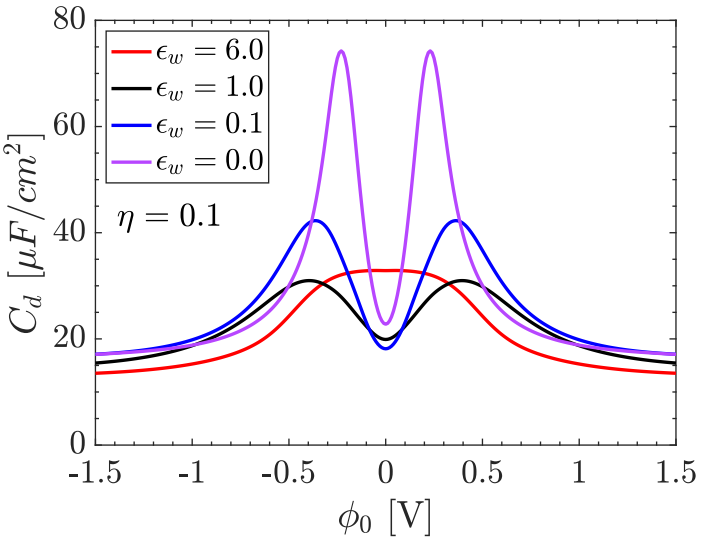

(b)

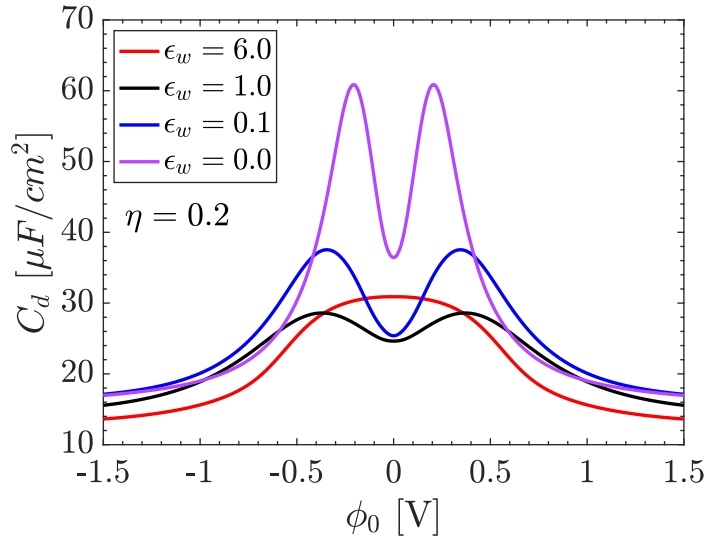

(c)

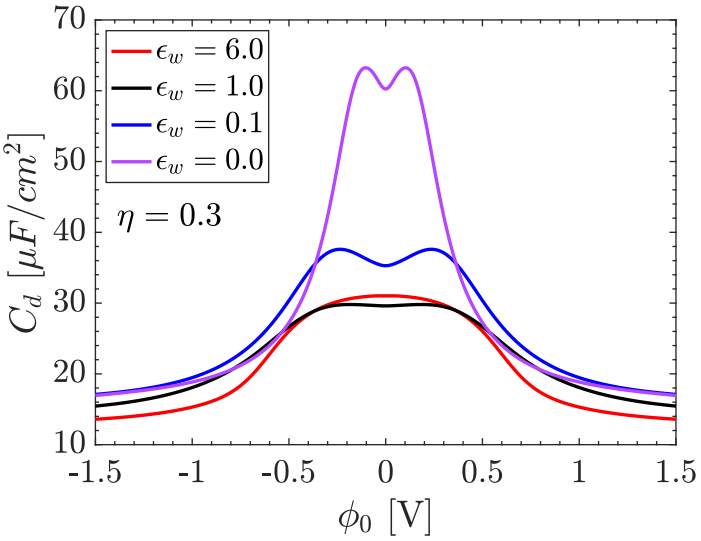

(d)

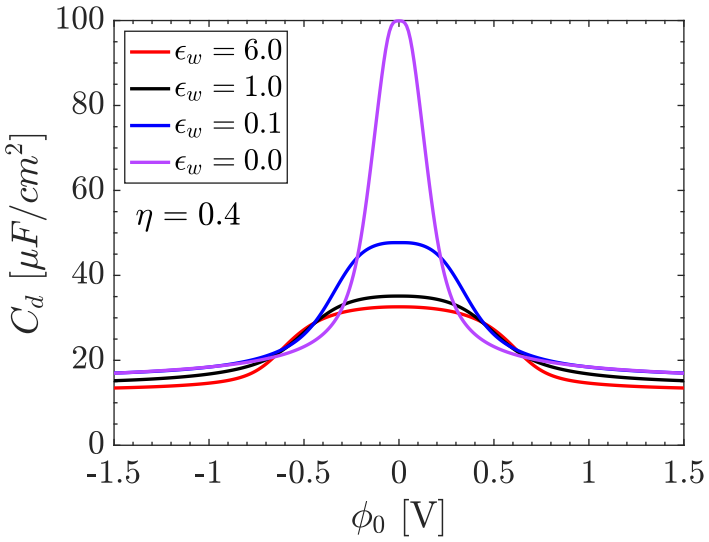

(e)

Figure 5.4: Differential capacitance as a function of electrode potential for packing fractions of $\eta = 0.05$ (a), $\eta = 0.1$ (b), $\eta = 0.2$ (c), $\eta = 0.3$ (d) and $\eta = 0.4$ (e). The plots are made for values of ϵ_w (in units of k_bT) of $\epsilon_w = 6$ (red), $\epsilon_w = 1$ (black), $\epsilon_w = 0.1$ (blue) and $\epsilon_w = 0$ (violet). All graphs are made for an inter-particle attraction strength of $\epsilon_p = 0.5k_bT$.

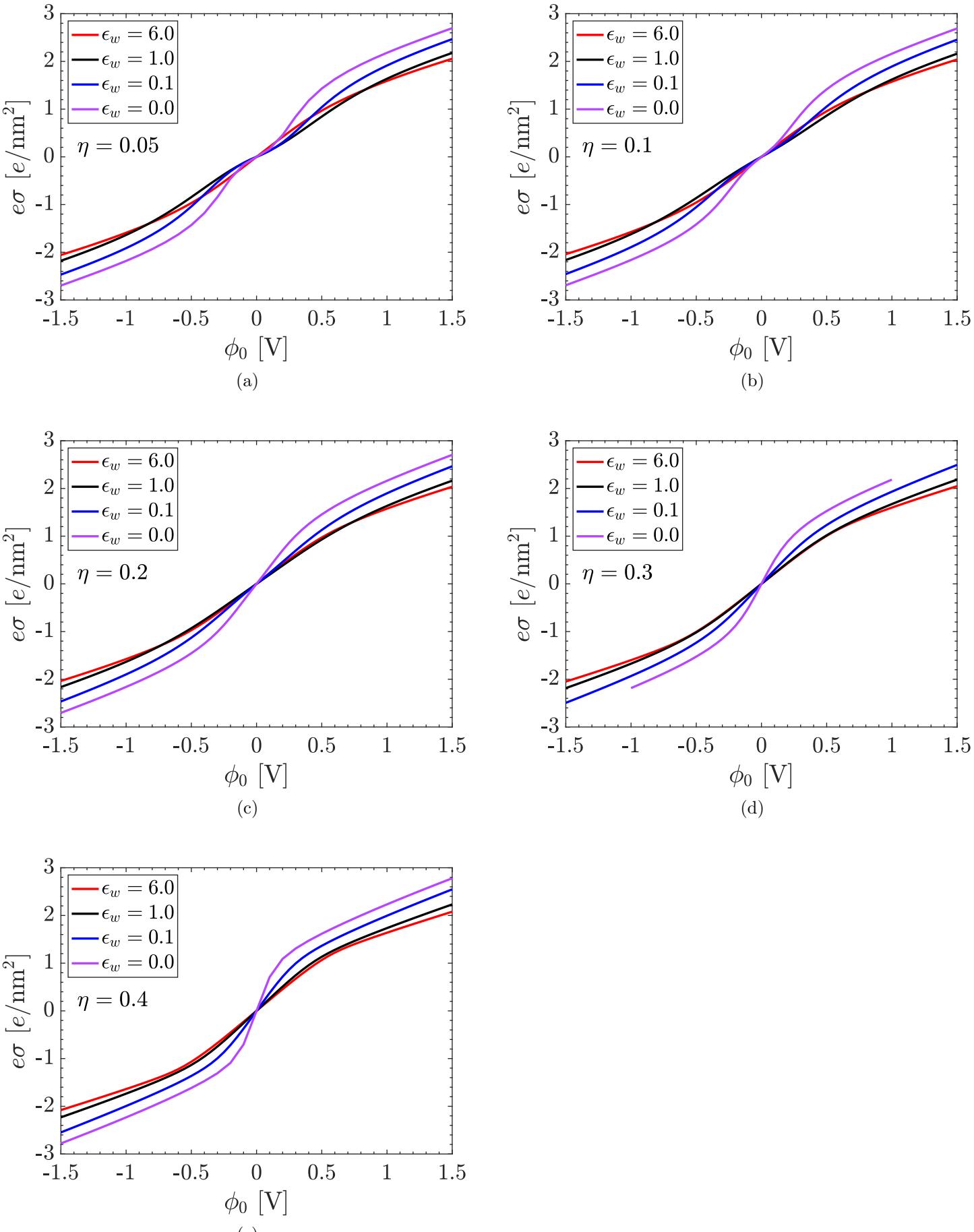

Figure 5.5: Surface charge densities as a function of the electrode potential for packing fractions of $\eta = 0.05$ (a), $\eta = 0.1$ (b), $\eta = 0.2$ (c), $\eta = 0.3$ (d) and $\eta = 0.4$ (e). The plots are made for values of ϵ_w (in units of k_bT) of $\epsilon_w = 6$ (red), $\epsilon_w = 1$ (black), $\epsilon_w = 0.1$ (blue) and $\epsilon_w = 0$ (violet). All graphs are made for an inter-particle attraction strength of $\epsilon_p = 0.0k_bT$.

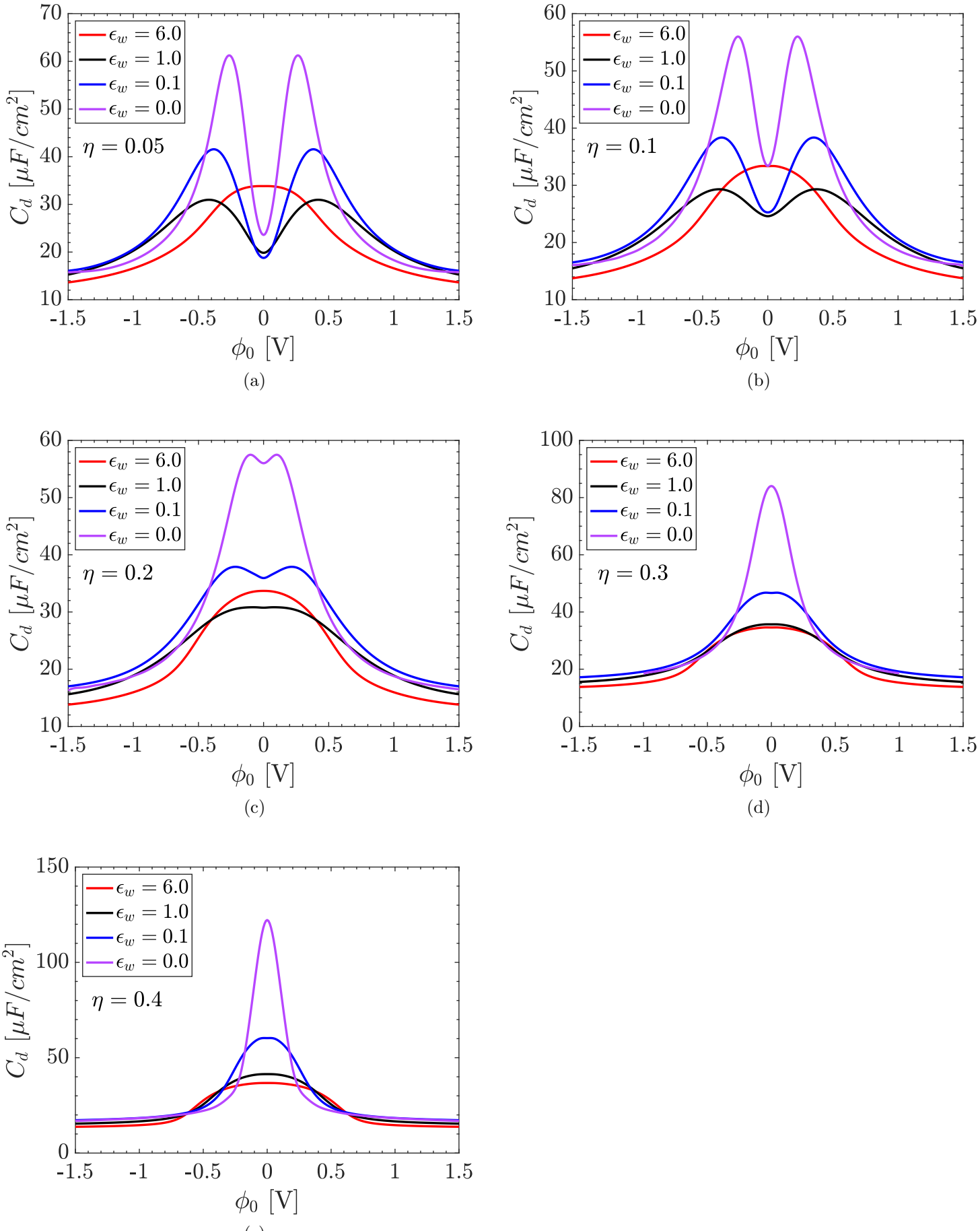

Figure 5.6: Differential capacitance as a function of electrode potential for packing fractions of $\eta = 0.05$ (a), $\eta = 0.1$ (b), $\eta = 0.2$ (c), $\eta = 0.3$ (d) and $\eta = 0.4$ (e). The plots are made for values of ϵ_w (in units of k_bT) of $\epsilon_w = 6$ (red), $\epsilon_w = 1$ (black), $\epsilon_w = 0.1$ (blue) and $\epsilon_w = 0$ (violet). All graphs are made for an inter-particle attraction strength of $\epsilon_p = 0.0k_bT$.

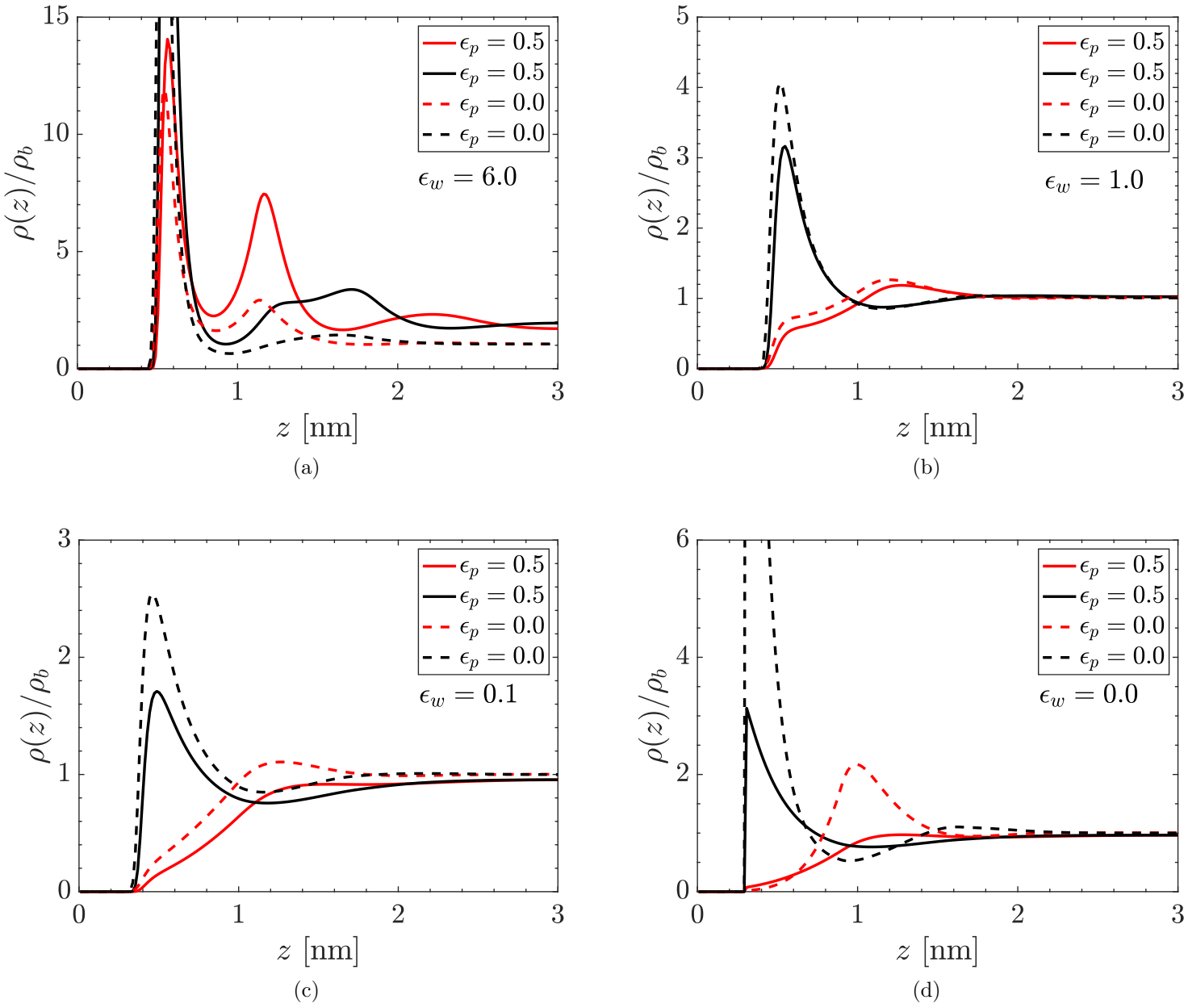

Figure 5.7: Cationic and anionic density profiles normalized to bulk density for an electrode potential of 0.1 V and a packing fraction of $\eta = 0.05$. The values for the energy parameter ϵ_w are $\epsilon_w = 6$ (a), $\epsilon_w = 1$ (b), $\epsilon_w = 0.1$(c) and $\epsilon_w = 0$ (d). The red lines indicate co-ions, and the black lines counter-ions. The dashed lines indicate that $\epsilon_p = 0$ while the solid lines indicate that $\epsilon_p = 0.5$.

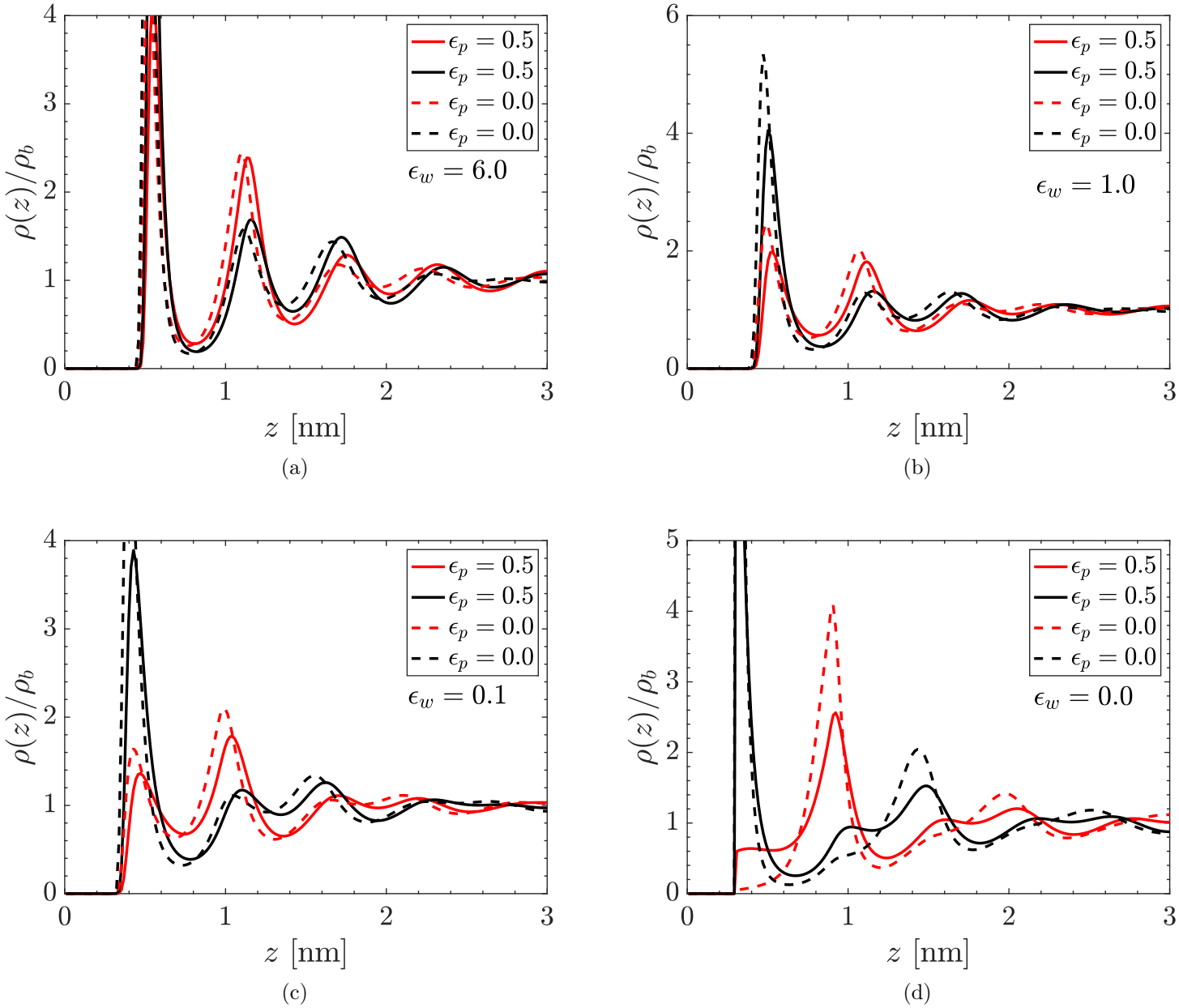

Figure 5.8: Cationic and anionic density profiles normalized to bulk density for an electrode potential of 0.1 V and a packing fraction of $\eta = 0.4$. The values for the energy parameter ϵ_w are $\epsilon_w = 6$ (a), $\epsilon_w = 1$ (b), $\epsilon_w = 0.1$(c) and $\epsilon_w = 0$ (d). The red lines indicate co-ions, and the black lines counter-ions. The dashed lines indicate that $\epsilon_p = 0$ while the solid lines indicate that $\epsilon_p = 0.5$.

Bibliography

[1] Murphy, O., Srinivasan, S. and Conway, B. (n.d.). *Electrochemistry in Transition.*

[2] Janssen, M. The electric double layer put to work; thermal physics at electrochemical interfaces. PhD thesis. Utrecht University.

[3] Watanabe, M., Thomas, M., Zhang, S., Ueno, K., Yasuda, T. and Dokko, K. (2017). Application of Ionic Liquids to Energy Storage and Conversion Materials and Devices. *Chemical Reviews*, 117(10), pp.7190-7239.

[4] Wishart, J. (2009). Energy applications of ionic liquids. *Energy and Environmental Science*, 2(9), p.956.

[5] van Roij, R. *Soft Condensed Matter Theory.* Lecture notes. Utrecht University.

[6] Evans, R. (1979). The nature of the liquid-vapour interface and other topics in the statistical mechanics of non-uniform, classical fluids. *Advances in Physics*, 28(2), pp.143-200.

[7] Roth, R. *Introduction to Classical Density Functional Theory.* Lecture notes. Stuttgart University.

[8] Härtel, A. *Density functional theory of hard colloidal particles: From bulk to interfaces.* PhD thesis. Heinrich-Heine Universität Düsseldorf.

[9] Bongsoo, K. *Density Functional Theory for Inhomogeneous fluids.* Lecture notes. Changwong National University, Korea.

[10] Hansen, J. and McDonald, I. (n.d.). *Theory of simple liquids.*

[11] Hohenberg, P. and Kohn, W. (1964). Inhomogeneous Electron Gas.*Physical Review*, 136(3B), pp.B864-B871.

[12] Mermin, N. (1965). Thermal Properties of the Inhomogeneous Electron Gas. *Physical Review*, 137(5A), pp.A1441-A1443.

[13] Rosenfeld, Y. (1988). Scaled field particle theory of the structure and the thermodynamics of isotropic hard particle fluids. *The Journal of Chemical Physics*, 89(7), pp.4272-4287.

[14] Tarazona, P. (2000). Density Functional for Hard Sphere Crystals: A Fundamental Measure Approach. *Physical Review Letters*, 84(4), pp.694-697.

[15] Yu, Y. (2009). A novel weighted density functional theory for adsorption, fluid-solid interfacial tension, and disjoining properties of simple liquid films on planar solid surfaces. *The Journal of Chemical Physics, 131(2), p.024704.*

[16] Robledo, A. and Varea, C. (1981). On the relationship between the density functional formalism and the potential distribution theory for nonuniform fluids. *Journal of Statistical Physics*, 26(3), pp.513-525.

[17] Roth, R. and Gillespie, D. (2017). Corrigendum: Shells of charge: a density functional theory for charged hard spheres (2016 J. Phys. Condens. Matter 28 244006). *Journal of Physics: Condensed Matter*, 29(44), p.449501.

[18] Hansen-Goos, H. and Roth, R. (2006). Density functional theory for hard-sphere mixtures: the White Bear version mark II. *Journal of Physics: Condensed Matter*, 18(37), pp.8413-8425.

[19] Weingärtner, H. (2014). The static dielectric permittivity of ionic liquids. *Journal of Molecular Liquids*, 192, pp.185-190.

[20] Siderius, D. and Gelb, L. (2011). Extension of the Steele 10-4-3 potential for adsorption calculations in cylindrical, spherical, and other pore geometries. *The Journal of Chemical Physics*, 135(8), p.084703.

[21] Tang, Y. and Wu, J. (2003). A density-functional theory for bulk and inhomogeneous Lennard-Jones fluids from the energy route. *The Journal of Chemical Physics*, 119(14), pp.7388-7397.

[22] Zhang, Q., Han, Y., Wang, Y., Ye, S. and Yan, T. (2014). Comparing the differential capacitance of two ionic liquid electrolytes: Effects of specific adsorption. *Electrochemistry Communications*, 38, pp.44-46.

[23] Jitvisate, M. and Seddon, J. (2017). Direct Measurement of the Differential Capacitance of Solvent-Free and Dilute Ionic Liquids. *The Journal of Physical Chemistry Letters*, 9(1), pp.126-131.

[24] Lamperski, S., Outhwaite, C. and Bhuiyan, L. (2009). The Electric Double-Layer Differential Capacitance at and near Zero Surface Charge for a Restricted Primitive Model Electrolyte. *The Journal of Physical Chemistry B*, 113(26), pp.8925-8929.

[25] Fedorov, M. and Kornyshev, A. (2008). Ionic Liquid Near a Charged Wall: Structure and Capacitance of Electrical Double Layer. *The Journal of Physical Chemistry B*, 112(38), pp.11868-11872.

[26] Jiang, D., Meng, D. and Wu, J. (2011). Density functional theory for differential capacitance of planar electric double layers in ionic liquids. *Chemical Physics Letters*, 504(4-6), pp.153-158.

[27] Lauw, Y., Horne, M., Rodopoulos, T. and Leermakers, F. (2009). Room-Temperature Ionic Liquids: Excluded Volume and Ion Polarizability Effects in the Electrical Double-Layer Structure and Capacitance. *Physical Review Letters*, 103(11).

[28] Vatamanu, J., Borodin, O. and Smith, G. (2010). Molecular Insights into the Potential and Temperature Dependences of the Differential Capacitance of a Room-Temperature Ionic Liquid at Graphite Electrodes. *Journal of the American Chemical Society*, 132(42), pp.14825-14833.

[29] Loth, M., Skinner, B. and Shklovskii, B. (2010). Anomalously large capacitance of an ionic liquid described by the restricted primitive model. *Physical Review E*, 82(5).

[30] Trulsson, M., Algotsson, J., Forsman, J. and Woodward, C. (2010). Differential Capacitance of Room Temperature Ionic Liquids: The Role of Dispersion Forces. *The Journal of Physical Chemistry Letters*, 1(8), pp.1191-1195.

[31] Fedorov, M. and Kornyshev, A. (2008). Towards understanding the structure and capacitance of electrical double layer in ionic liquids. *Electrochimica Acta*, 53(23), pp.6835-6840.

[32] Lockett, V., Sedev, R., Ralston, J., Horne, M. and Rodopoulos, T. (2008). Differential Capacitance of the Electrical Double Layer in Imidazolium-Based Ionic Liquids: Influence of Potential, Cation Size, and Temperature. *The Journal of Physical Chemistry C*, 112(19), pp.7486-7495.

[33] Alam, M., Mominul Islam, M., Okajima, T. and Ohsaka, T. (2007). Measurements of differential capacitance in room temperature ionic liquid at mercury, glassy carbon and gold electrode interfaces. *Electrochemistry Communications*, 9(9), pp.2370-2374.

[34] Filion, L. and van Roij, R. *Advanced Statistical Physics*. Lecture notes. Utrecht University.

[35] Blundell, S. and Blundell, K. *Concepts in thermal Physics*. Oxford University Press, 2010.

[36] Olver, P. On the calculus of variations. Lecture notes. University of Minnesota. 2019. http://www-users.math.umn.edu/~olver/ln_/cv.pdf

[37] Zia, R,. Redish, E. and Mckay, S. *Making sense of the legendre transform*. https://arxiv.org/abs/0806.1147.

[38] Campisi, M. and Kobe, D. (2010). Derivation of the Boltzmann principle. *American Journal of Physics*, 78(6), pp.608-615.

Appendix A

Calculus of variations

In the field of mathematical analysis a functional refers to a mapping from a space X (for all intends and purposes with a topology induced by a suitable inner product) into the real numbers $\mathbb{R}$. Commonly, and always in the discussion following in this section, the space X is a space of functions defined on some (subset) of euclidean space. In other words, a functional assigns to every *function* $f \in X$ a real number $r \in \mathbb{R}$.

Calculus of variations is the area of mathematics concerned with finding extrema of functionals. Like in calculus, where one is concerned with points that extremize a *function*, we are on a quest to find *functions* extremizing a *functional*. As history has shown, minimization problems that can be analyzed by means of calculus of variations pop up all over physics. Since this will also be a topic of importance in this thesis, the basics will be discussed here.

A simple yet illustrative problem that can be solved by making use of the calculus of variations is finding the curve that minimizes the distance between two arbitrary points $(a, y), (b, y') \in \mathbb{R}^2$. More precisely, denote $X = \{f \in C^\infty[a, b] | f(a) = y, f(b) = y'\}$, where we have used the standard notation $C^\infty[a, b]$ to denote the class of continuously differentiable functions defined on $[a, b]$ with target $\mathbb{R}$. The arc length of f is given by $J(f) = \int_a^b \sqrt{1 + (f'(x))^2} dx$. Clearly, $J : C^\infty[a, b] \to \mathbb{R}$ satisfies the above characterization of a functional. Now the technique of calculus of variations provides a tool for finding the function $f \in X$ that minimizes the functional. In other words, the function f is the function of which the arc length between the two points in question is minimal. It is not hard to show that the function accomplishing this is a straight line, in accordance with ones intuition.

We will introduce the variational techniques on a rather informal manner and focus primarily on the simple class of problems where the functions are at least twice continuously differentiable scalar functions and where the functional to be minimized depends on mostly the first derivative. This introduction mainly follows the set of lecture notes [36].

We will consider the following objective functional

$$J[y] = \int_a^b L(x, y(x), y'(x)) dx, \tag{A.1}$$

where $L(x, y(x), y'(x))$ is commonly referred to as the *Lagrangian* and is assumed to be reasonably (say, twice continuously differentiable) smooth with respect to its arguments

(observe that its arguments also consist of *functions*, we regard the differentiation as if those functions were ordinary variables). From ordinary calculus we recall the definition of the directional derivative of a function f that is differentiable in $(x_1, \cdots, x_n)$

$$\nabla_v f(x_1, x_2, \cdots, x_n) := \langle \nabla f(x_1, \cdots, x_n), \mathbf{v} \rangle. \tag{A.2}$$

For simplicity we will consider the L^2 inner product on the function space, which is given by

$$\langle \cdot, \cdot \rangle : C^2[a, b] \to \mathbb{R}, \langle f, g \rangle = \int_a^b f(x)g(x)dx. \tag{A.3}$$

In analogy with ordinary calculus we now compute

$$\langle \nabla J[y], v \rangle = \frac{d}{d\epsilon} J[y + \epsilon v]|_{\epsilon=0}, \tag{A.4}$$

where ϵv is known as the *variation* in the function y and also commonly denoted by δy. Now simply inserting Eq. (A.1) into Eq. (A.4) and invoking the chain rule yields

$$\begin{aligned}
\langle \nabla J[y], v \rangle &= \frac{d}{d\epsilon} J[y + \epsilon v]|_{\epsilon=0} = \int_a^b \frac{d}{d\epsilon} L(x, y + \epsilon v, y' + \epsilon v')dx|_{\epsilon=0} \\
&= \int_a^b [v \frac{\partial L}{\partial y}(x, y + \epsilon v, y' + \epsilon v) + v' \frac{\partial L}{\partial y'}(x, y + \epsilon v, y' + \epsilon v')]dx|_{\epsilon=0} \\
&= \int_a^b [v \frac{\partial L}{\partial y}(x, y, y') + v' \frac{\partial L}{\partial y'}(x, y, y')]dx \\
&= \int_a^b v \frac{\partial L}{\partial y}(x, y, y') + \frac{d}{dx}(\frac{\partial L}{\partial y'} v) - v \frac{d}{dx} \frac{\partial L}{\partial y'} dx \\
&= \int_a^b v \frac{\partial L}{\partial y} - v \frac{d}{dx} \frac{\partial L}{\partial y'} dx + \frac{\partial L}{\partial y'} v|_a^b,
\end{aligned} \tag{A.5}$$

where in the last step we have integrated by parts. Since $v(x)$ was chosen arbitrarily we have our desired expression,

$$\nabla J[y] = \frac{\partial L}{\partial y}(x, y, y') - \frac{d}{dx}(\frac{\partial L}{\partial y'}(x, y, y')), \tag{A.6}$$

to which we will refer as the functional derivative of the functional in Eq. (A.1). In analogy with ordinary calculus, we will refer to *critical functions* as functions $y(x)$ for which the functional derivative vanishes. In its full glory this is a second order ordinary differential equation going by the name of *Euler-Lagrange equation*

$$\frac{\partial L}{\partial y} - \frac{\partial^2 L}{\partial x \partial y'} - y' \frac{\partial^2 L}{\partial y \partial y'} - y'' \frac{\partial^2 L}{\partial y'^2} = 0 \tag{A.7}$$

Appendix B

Thermodynamics

In order to give a complete description of a piece of macroscopic matter one would need to specify the coordinates of all constituent particles. The order of magnitude for this set of coordinates is 10^{23}, commonly referred to as Avogadro's number. It would be a futile task describing macroscopic materials in this way.

The study of classical thermodynamics is not concerned with studying the individual degrees of freedom of the constituents of a bulk of matter, but rather with those characteristics of a system that arise as means when looking at the statistical behaviour of many particles, like pressure and temperature.

A brief overview of thermodynamics will be provided here, mainly following the introductory pages of [34] and [5]. For a slightly more thorough review we refer to [35]. In this section a *system* will be whatever part of the universe we are considering. Its *surroundings* will be the complement of the system.

B.0.1 Intensive and extensive variables and work

A thermodynamic variable is referred to as being *extensive* whenever it scales linearly with system size. In contrast, and *intensive* when it does not scale with system size. Examples of extensive variables are volume, V, and number of particles, N. An example of intensive variables are temperature T and pressure p.

The work done on a system is defined by $\delta W = \mathbf{f} \cdot d\mathbf{X}$. Here $\mathbf{f}$ is a generalized force (e.g. pressure or chemical potential) and $\mathbf{X}$ is the changing extensive variable associated with $\mathbf{f}$ (e.g. volume or number of particles). The δ means that the work depends on the path taken between initial and final states, and not just on the initial and final state itself.

B.0.2 The first law

The first law of thermodynamics states that energy in closed systems is conserved. It is possible to transform between different forms of energy, but it is not possible to create or destroy energy. The internal energy of a system can change by work performed either on or by the system, or by means of transferring heat. In differential form we can state the first law as

$$dU = \delta Q + \delta W, \tag{B.1}$$

where dU denotes the change in internal energy, δQ is the heat transferred *to* the system and δW is the work done *on* the system. We note that the internal energy is a so called *function of state* meaning that a system in equilibrium has a fixed, definite, value for U independent on the path taken from initial to final state. Compare this with δQ, δW, where the δ's indicate that the work and heat added to a system depend on the path taken (that is, the path from the initial state to the final state).

B.0.3 The second law

The second law of thermodynamics states that the entropy of a closed system can never spontaneously decrease. This is reflected in the fact that processes in nature follow the arrow of time. In other words, while it is not forbidden by the first law for your ice cream to cool the sun, we only observe the sun heating up our ice cream. There are, however, many equivalent ways of stating the second law. Lords Kelvins definition of the second law is that processes that convert heat into work with 100% efficiency cannot occur.

In order to formally introduce the concept of entropy and the second law, we introduce the notion of *reversibility* and *irreversibility*. A process that happens along a path from A to B is referred to as being reversible whenever the process can be reversed by performing infinitesimal changes to the system. The change takes place sufficiently slow for the system to be in constant internal equilibrium during the entire process. A textbook example of a reversible process would be the slow compression of a gas in a container, allowing the pressure to remain uniform when applying the (infinitesimal) changes to the volume. Any process that is not reversible is *irreversible*.

Mathematically the entropy is defined as the following state function

$$dS = \frac{dQ_{rev}}{T}, \tag{B.2}$$

where dQ_{rev} is a reversibly taken up amount of heat.

B.0.4 Thermodynamic potentials

The state variables describing the thermodynamic properties of a system are not independent. Depending on the situation it will be useful to convert between different *thermodynamic ensembles*. In this context, an ensemble is just the set of variables that are needed in order to fully specify the thermodynamics of the system. To every thermodynamic ensemble we can assign a potential, that is, a form of energy. For a simple system consisting of one component the total work δW in Eq. (B.1) is given by $\delta W = -pdV + \mu dN$, assuming the work is performed in a reversible manner. If the heat δQ in Eq. (B.1) is also taken up reversibly we can combine Eq. (B.1) and Eq. (B.2) and obtain the identity

$$dU = TdS - pdV + \mu dN. \tag{B.3}$$

Now we note that dS, dV and dN are functions of state. Hence Eq. (B.3) holds for any process given that there *exists* a reversible path between the initial and the final

states. Equation (B.3) corresponds to an isolated system, where entropy S, volume V and number of particles N are fixed. The potential assigned to this S, V, N**-ensemble** is the internal energy U

The meaning of Eq. (B.3) is not to be underestimated. Knowledge of $U(S, V, N)$ yields all the thermodynamic information of the system in question through the set of equations

$$T = \left(\frac{\partial U}{\partial S}\right)_{V,N}, p = -\left(\frac{\partial U}{\partial V}\right)_{S,N}, \mu = \left(\frac{\partial U}{\partial N}\right)_{S,V}. \tag{B.4}$$

In many situations, however, Eq. (B.3) is not very practical to work with. It is imaginable that in a experiment for example it is not always convenient to control the entropy. In order to circumference this practical problem we can use Legendre transformations to construct functions of other thermodynamical variables. The details will be omitted in this discussion. For a in-depth explanation of Legendre transformations see [37].

The N, V, T-ensemble

The relevant energy in this ensemble is known as the Helmholtz free energy, denoted $F = U - TS$ which differential form is given by

$$dF = dU - TdS - SdT = -SdT - pdV + \mu dN. \tag{B.5}$$

The thermodynamics follows from the set of equations:

$$S = -\left(\frac{\partial F}{\partial T}\right)_{V,N}, p = -\left(\frac{\partial F}{\partial V}\right)_{V,N}, \mu = \left(\frac{\partial F}{\partial N}\right)_{V,T}. \tag{B.6}$$

The N, P, T-ensemble The relevant energy in this ensemble is known as the Gibbs free energy, $G = U - TS + pV$, which differential form is

$$dG = dU - TdS - SdT + pdV + Vdp. \tag{B.7}$$

The thermodynamics follows from the set of equations:

$$S = -\left(\frac{\partial G}{\partial T}\right)_{p,N}, V = \left(\frac{\partial G}{\partial p}\right)_{V,N}, \mu = \left(\frac{\partial G}{\partial N}\right)_{p,T}. \tag{B.8}$$

The μ, V, T-ensemble

The relevant energy in this ensemble is known as the grand potential Ω, which differential form is given by

$$d\Omega = -SdT - pdV - Nd\mu. \tag{B.9}$$

The relevant thermodynamics follows from the set of equations:

$$S = -\left(\frac{\partial \Omega}{\partial T}\right)_{V,\mu}, p = -\left(\frac{\partial \Omega}{\partial V}\right)_{T,\mu}, N = -\left(\frac{\partial \Omega}{\partial \mu}\right)_{T,V}. \tag{B.10}$$

Appendix C

Statistical Physics

Statistical mechanics is one of the cornerstones of modern physics. It uses statistical methods and probability theory in combination with the microscopic physical laws governing 10^{23} degrees of freedom to describe systems. As it turns out, this powerful tool relates the concepts of macroscopic state variables (such as temperature, pressure, volume, etc) to descriptions of the microscopic state of a system and fluctuations around averages. Hence, it can be used to deduct the thermodynamic behaviour of systems with a large number of degrees of freedom. In this section we will introduce the relevant notions for so called classical fluids. For convenience we will assume that we are dealing with systems that consist of just one species of particle. Classical fluids are systems of particles for which the thermal (or De Broglie) wavelength $\Lambda = \frac{h}{\sqrt{2\pi m k_b T}}$ is much smaller than the atomic spacing. Here, h is the constant of Planck, m is the mass of the particle, k_b is Boltzmann's constant and T is the temperature. The fact that the thermal wavelength is much less than the particle spacing means that we do not have to take into consideration quantum effects.

C.0.1 Phase space and the Liouville equation

In the second half of the 19th century famous mathematicians and physicists Ludwig Boltzmann, Henri Poincaré and Josiah Gibbs were working on the concept of *phase space*. Given a system, a phase space is a (usually Euclidean) space in which every degree of freedom of the system has its own coordinate axis. Every physically allowed state of the system is thus represented by a point in this space, called a *phase point*.

As an example consider N identical classical particles confined to a three dimensional volume V. If we assume that the only degrees of freedom of a particle are translational a phase point Γ in the phase space $\mathcal{P}$ can be characterized by $3N$ spatial coordinates and $3N$ momenta of the particles. The conserved energy of the system expressed in terms of coordinates and momenta is called the *Hamiltonian*. In this case the Hamiltonian takes the form

$$H(\mathbf{r_1} \cdots \mathbf{r_N}, \mathbf{p_1}, \cdots, \mathbf{p_N}) = \sum_{i=1}^{N} \frac{\mathbf{p_i^2}}{2m} + \Phi(\mathbf{r_1} \cdots \mathbf{r_N}). \tag{C.1}$$

Here $\{\mathbf{r}_i\}_{i\in\{1,\cdots N\}}$ denotes the position of the i'th particle and $\{\mathbf{p}_i\}_{i\in\{1,\cdots N\}}$ denotes the momentum of the i'th particle. Having the Hamiltonian one can write Newtons equations

of motion in the following form

$$\dot{\mathbf{r}}_i = \frac{\partial H}{\partial \mathbf{p}_i}, \quad \dot{\mathbf{p}}_i = -\frac{\partial H}{\partial \mathbf{r}_i}, \tag{C.2}$$

referred to as the Hamilton equations of motion. The dot on top of a coordinate stands for the derivative with respect to time.

In this context we can make the definition of an ensemble a bit more precise. We can define an ensemble as a collection of phase points with the same macroscopic properties. In other words, we are considering a large number of snapshots of the system, in which every degree of freedom is specified, all at once (where the snapshots have the same macroscopic properties). At a given time t an ensemble consists of a collection of points in phase space. The distribution of these points is determined by the phase space probability density $f(\Gamma, t)$, where $f(\Gamma, t)d\Gamma$ is the probability to find the system in a microscopic state characterized by its location in the infinitesimal volume element $d\Gamma$ around Γ in phase space.

The time evolution of a probability density $f(\Gamma, t)$ is determined by the so called Liouville equation

$$\frac{\partial f}{\partial t} + \frac{\partial}{\partial \Gamma}(\dot{\Gamma} f(\Gamma, t)) = 0. \tag{C.3}$$

C.0.2 Effective Hamiltonians

In the statistical physics description of materials we often consider molecules, atoms or ions. Other higher energy contributions (due to atomic constituents like electrons) are not taken into consideration. The Hamiltonians of the classical fluids we consider always take the following form

$$H_{cl} = \sum_{i=1}^{N} \frac{\mathbf{p}_i}{2m} + \Phi + \text{some external potential}, \tag{C.4}$$

where the first term is the kinetic energy of particle i and the second term is the interparticle potential. In the theoretical description of classical fluids it is mostly assumed that the interparticle potential Φ is pairwise additive, meaning that Φ becomes a sum of some pair potential $\phi(|\mathbf{r}_i - \mathbf{r}_j|)$ that depends only on the radial distance between particles i and j. Fluids for which the potential is pairwise are often called *simple*. A commonly used, and quite famous, parameterization for ϕ is the *Lennard-Jones* (LJ) potential

$$\phi_{LJ}(r) = 4\epsilon \left(\left(\frac{\sigma}{r}\right)^{12} - \left(\frac{\sigma}{r}\right)^{6} \right), \tag{C.5}$$

where the r^{-12} term describes the short-ranged repulsion due to Pauli exclusion and the r^6 term describes the long range attractions due to dipole-dipole induced interactions. Here, ϵ is the strength of the potential well and σ is a measure for the finite distance at which the interparticle interaction is zero.

A similar but more crude form of the pair potential is given by the square well (SW) and hard sphere (HS) potentials

$$\phi_{SW} = \begin{cases} \infty & r \leq \sigma \\ -\epsilon & \sigma < r < \lambda\sigma \\ 0 & r > \lambda\sigma, \end{cases} \tag{C.6}$$

where λ is a parameter introduced as a measure for the range of the attractive well. The simplest repulsive pair potential is the hard-sphere (HS) potential,

$$\phi_{HS} = \begin{cases} \infty & r \leq \sigma \\ 0 & r > \sigma. \end{cases} \tag{C.7}$$

In the hard-sphere potential there is no attraction term, seemingly unphysical. But as it turns out the hard-sphere potential is extremely useful in many approximations, especially as a reference point in thermodynamic perturbation theory. In the theoretical development we will make frequent use of the hard sphere repulsion terms (also known as steric interactions).

C.0.3 Classical ensembles

We have already seen that t different ensembles exist distinguished by the thermodynamic variables that are conserved. Here we will explore this notion further and consider three statistical ensembles that are of particular interest, the *microcanonical ensemble*, the *canonical ensemble* and the *grand canonical ensemble*.

In the microcanonical ensemble we consider a collection of phase points where the energy U, volume V and number of particles N are all fixed. Consequently the phase space distribution function for this ensemble is given by a Dirac-delta distribution

$$f_m(\Gamma) = \frac{\delta(U - H(\Gamma))}{\omega(U, V, N)}, \tag{C.8}$$

$$\omega(U, V, N) = \int d\Gamma \delta(U - H(\Gamma)). \tag{C.9}$$

Here, Eq. (C.9) enforces the normalisation constraint. Note that the probability distribution depends only on the total energy of the system. The link to thermodynamics is given by the famous *Boltzmann equation*

$$S(U, V, N) = k_B \log \frac{\omega(U, V, N)}{N! h^{3N}}, \tag{C.10}$$

with k_B the Boltzmann constant, h Planck's constant and $N!$ a counting factor in order to make the entropy extensive. For a derivation of this formula one can have a look at [38].

The canonical ensemble describes the equilibrium properties of a system that can exchange energy with a reservoir at a fixed temperature T. Furthermore, V and N remain fixed. In this case the distribution of energies is governed by the Boltzmann-distribution and the phase space distribution function takes the following form

$$f_c(\Gamma) = \frac{e^{-\beta H(\Gamma)}}{N! h^{3N} Z(N, V, T)}. \tag{C.11}$$

Here $\beta = \frac{1}{k_B T}$ is the inverse temperature and $Z(N, V, T)$ denotes the canonical partition function

$$Z(N, V, T) = \frac{1}{N! h^{3N}} \int d\Gamma e^{-\beta H(\Gamma)}. \tag{C.12}$$

The link to thermodynamics is given by the following relation between the Helmholtz free energy and the partition function:

$$F(N, V, T) = -k_B T \log(Z(N, V, T)). \tag{C.13}$$

The grand canonical ensemble describes the equilibrium properties of a system that can exchange both energy and particles at fixed temperature T, volume V and chemical potential μ. The grand canonical partition sum takes on the form

$$f_g(\Gamma) = \frac{e^{-\beta(H(\Gamma) - \mu N}}{N! h^{3N} \Xi(\mu, V, T)}, \tag{C.14}$$

with the grand canonical partition function

$$\Xi(\mu, V, T) = \sum_{N=0}^{\infty} \frac{e^{\beta N \mu}}{N! h^{3N}} \int d\Gamma e^{-\beta H(\Gamma)}. \tag{C.15}$$

The link to thermodynamics is given by relating the grand canonical partition function to the relevant potential in the ensemble

$$\Omega(\mu, T, V) = -k_B T \log(\Xi(\mu, V, T)). \tag{C.16}$$

Appendix D

Picard-iteration Scheme

We recall here the self consistent equation for the density profile that DFT predicts

$$\rho(\mathbf{r}) = \rho_{bulk} \exp[-\beta V_{ext}(\mathbf{r}) + c^{(1)}(\mathbf{r}) + \beta\mu_{ext}] \tag{D.1}$$

Where $c^{(1)}$ is the one body direct correlation function

$$c^{(1)}(\mathbf{r}) = -\beta \frac{\delta \mathcal{F}_{ex}[\rho]}{\delta \rho} \tag{D.2}$$

At this point $\mathcal{F}_{ex}$ is just the general excess free energy functional. The code can take into account Lennard-Jones interactions, coulombic interactions between ions and charged walls and short ranged hard-core repulsion. The Picard-iteration method used to solve this equation can be summarized in four steps.

1. Initialize the density profile $\rho^0(z)$. In our case often a flat profile is used.
2. Calculate ρ'^1 using the self-consistency equation with the initial density profile.
3. Mix together the newly obtained solution with the old one with mixing parameter a: $\rho^{i+1}(z) = (1-a)\rho^{(i)}(z) + a\rho'^{(i)}$
4. Go back to the second step until the solution converges to the density profile